Energy, Mines and Resources Canada
Earth Physics Branch
1 Observatory Crescent
Ottawa Canada.
K1A 0Y3

Energie, Mines et Ressources Canada
Direction de la physique du globe
1 Place de l'Observatoire
Ottawa, Canada
K1A 0Y3

Geothermal Service of Canada

Service géothermique du Canada

AN INVESTIGATION OF THE DISTRIBUTION OF PERMAFROST ON THE SABINE PENINSULA OF MELVILLE ISLAND, N.W.T. AND ITS RELATIONSHIP TO GLACIAL AND SEA-LEVEL HISTORY

H. M. French and D. Desrochers
University of Ottawa

Earth Physics Branch Open File Number 82-7

Ottawa, Canada, 1982

Price/Prix: $25.00

Abstract

The distribution of permafrost, as determined from a number of observations of subsurface temperatures in abandoned oil wells, is related to the Holocene marine emergence of the Sabine Peninsula, Melville Island, N.W.T.

Résumé

La répartition du pergélisol, déterminée à partir d'un certain nombre d'observations des tempéératures souterraines dans des puits de pétrole abandonnés, est mise en relation avec l'émergence de la péninsule Sabine, dans l'île Melville, T.N.-O., au cours de l'Holocène.

FINAL REPORT

AN INVESTIGATION OF THE DISTRIBUTION OF PERMAFROST ON THE SABINE PENINSULA OF MELVILLE ISLAND, N.W.T. AND ITS RELATIONSHIP TO THE GLACIAL AND SEA-LEVEL HISTORY

Hugh M. French
Departments of Geography and Geology
University of Ottawa

May 1982

Contract Report, Contract OSU81-00160, Energy, Mines and Resources, Earth Physics Branch, Building No. 1, Observatory Crescent, Ottawa K1A 0Y3.

FINAL REPORT

During the period September 1981 - April 1982 the contract provided salary and other support to D. Desrochers, M.A. student in the Department of Geography.

As a first step towards understanding the permafrost distribution and thickness on the Sabine Peninsula, Desrochers focussed attention upon (a) available geothermal data held by the Earth Physics Branch, Energy Mines and Resources, for a number of abandoned wellsites on the Sabine Peninsula and (b) a literative review of the late-Quaternary history and geomorphology of the region. At the same time Desrochers successfully undertook the formal course requirements for the M.A. degree in Geography at the University of Ottawa. During the academic year 1982-83 Desrochers plans to prepare an M.A. thesis which will extend the present work.

Much time was spent between September and December 1981 in familiarisation with laboratory procedures at the Earth Physics Branch for the determination of thermal conductivity values. A Progress Report was submitted in early January 1982. Between January and April 1982, thermal conductivity values were obtained from a number of drill cutting samples which had been collected from seven wells on the Sabine Peninsula at the time of drilling. An attempt was then made to relate differences in permafrost temperatures

and thicknesses to variations in thermal conductivity values, to distance from sea, and time since marine emergence in Holocene times. Several numerical modelling procedures, developed at Earth Physics Branch, were applied to the data.

A paper entitled "Thermal conductivity measurements and permafrost conditions at wellsites on the Sabine Peninsula, Melville Island" has been prepared by D. Desrochers. This is attached to this report and summarises progress to date. A number of minor editorial changes have been made by the Principal Investigator, but the paper and results are primarily the work of Desrochers.

THERMAL CONDUCTIVITY MEASUREMENTS AND PERMAFROST CONDITIONS AT WELLSITES ON THE SABINE PENINSULA, EASTERN MELVILLE ISLAND

Daniel T. Desrochers
Department of Geography
University of Ottawa
Ottawa K1N 6N5

April 1982

TABLE OF CONTENTS

* * *

LIST OF FIGURES

* * *

LIST OF TABLES

* * *

1.

INTRODUCTION

The prediction of permafrost thickness requires knowledge of ground temperature gradient, thermal conductivity of the material, and the regional distribution of geothermal heat flow (Judge, 1973b). The present report describes measurements obtained from a divided-bar thermal conductivity apparatus, similar to that described in Beck (1957) for use with a cell containing rock fragments, for seven wells on the Sabine Peninsula of Melville Island (Drake D-73, Drake E-78, Drake D-68, Drake K-67A, Drake F-16, Drake B-44, Hecla I-69) (Figure 1). Five were measured by the author, and two (Drake B-44, Hecla I-69) by the Earth Physics Branch. Details of these wells are also given in Table 1.

In addition, results from heat flow determinations for five wells (Drake B-44, Drake E-78, Drake D-68, Drake D-73, and Hecla I-69) are outlined in order to establish a regional terrestrial heat flux. The latter may assist in the prediction of permafrost thicknesses on the Sabine Peninsula. An attempt is made to relate permafrost thickness and temperature at each site with known or measured thermal properties and geomorphic histories.

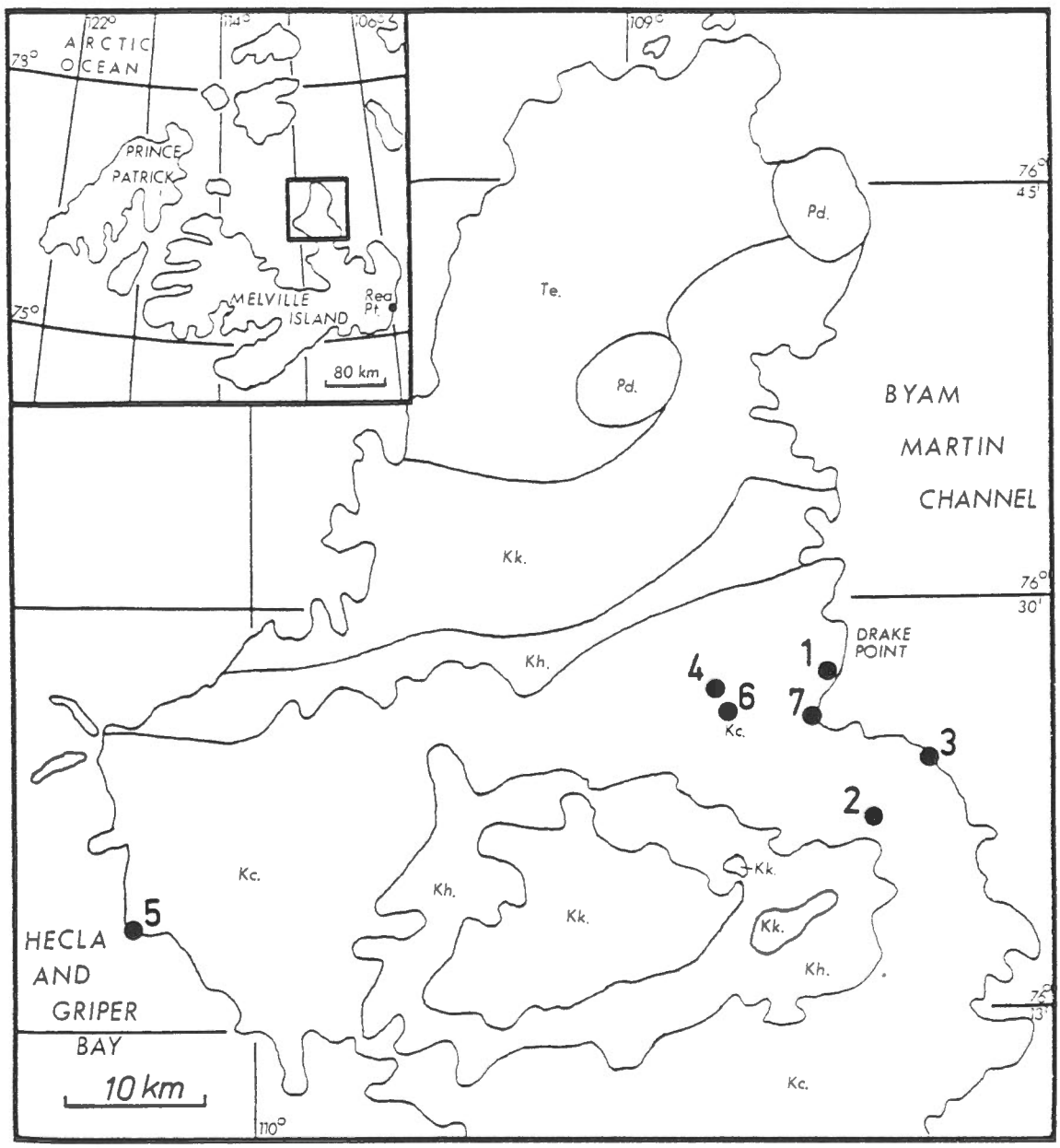

Figure 1. Location of wellsites chosen for study and geological boundaries, Sabine Peninsula, Eastern Melville Island.

1. Drake E-78.
2. Drake D-73.
3. Drake B-44.
4. Drake D-68.
5. Hecla I-69.
6. Drake K-67A.
7. Drake F-16.

Kc. Christopher Formation.
Kh. Hassel Formation.
Kk. Kanguk Formation.
Te. Eureka Sound Formation.
Pd. Piercement Domes.

Wellsites	Geographical Co-ordinates	Start and Completion Dates	Elevation (m a.s.l.)	Depth of Hole (m)	Thickness of Permafrost (m)
Drake E-78	76° 27.3'N 108° 29.4'W	74- 5- 2 74- 5-27	2	1356 (1221 vertical)	171
Drake D-73	76° 22.1'N 108° 29.5'W	75- 4-23 75- 5-10	33	1361	288
Drake B-44	76° 23.1'N 108° 16.1'W	72- 9-23 72-10-22	4	1396	188
Drake D-68	76° 27.1'N 108° 55.7'W	73- 6- 7 74- 5-25	37	5415	264
Drake K-67A	76° 26.4'N 108° 55.1'W	70- 7-19 70-11- 9	approx. 35	975	263*
Drake F-16	76° 25.2'N 108° 35.4'W	72- 5-10 72- 6-15	approx. 40	1478	200*
Hecla I-69	76° 18.7'N 110° 23.3'W	73- 2-27 73- 5- 9	2	1457	143

* no actual record, assumed thickness.

Table 1. Summary of wellsite data, Sabine Peninsula. Thermal conductivity measurements were made upon the seven wellsites. Hecla I-69 and Drake B-44 were measured by the Earth Physics Branch, and the five remaining sites by the author.

The wellsites were chosen because of the availability of ground temperature data obtained previously by the Earth Physics Branch. Permafrost temperatures near the surface on the Sabine Peninsula range between -16 and -19°C (Taylor and Judge, 1975; Taylor et al, 1982). Three of the wells examined in this report (Drake B-44, Drake E-78, and Hecla I-69) are at elevations of less than 5 m a.s.l. Permafrost thicknesses exceed 250 m at the two wellsites of high elevation (Drake D-68; Drake D-73). By contrast, at the three wellsites close to sea level, permafrost thicknesses are less than 200 m (Figure 2).

All seven wellsites can be described in terms of surficial deposits, vegetation, elevation above or below marine limit, and geomorphological processes operating in the vicinity. These data are indicated in Table 2.

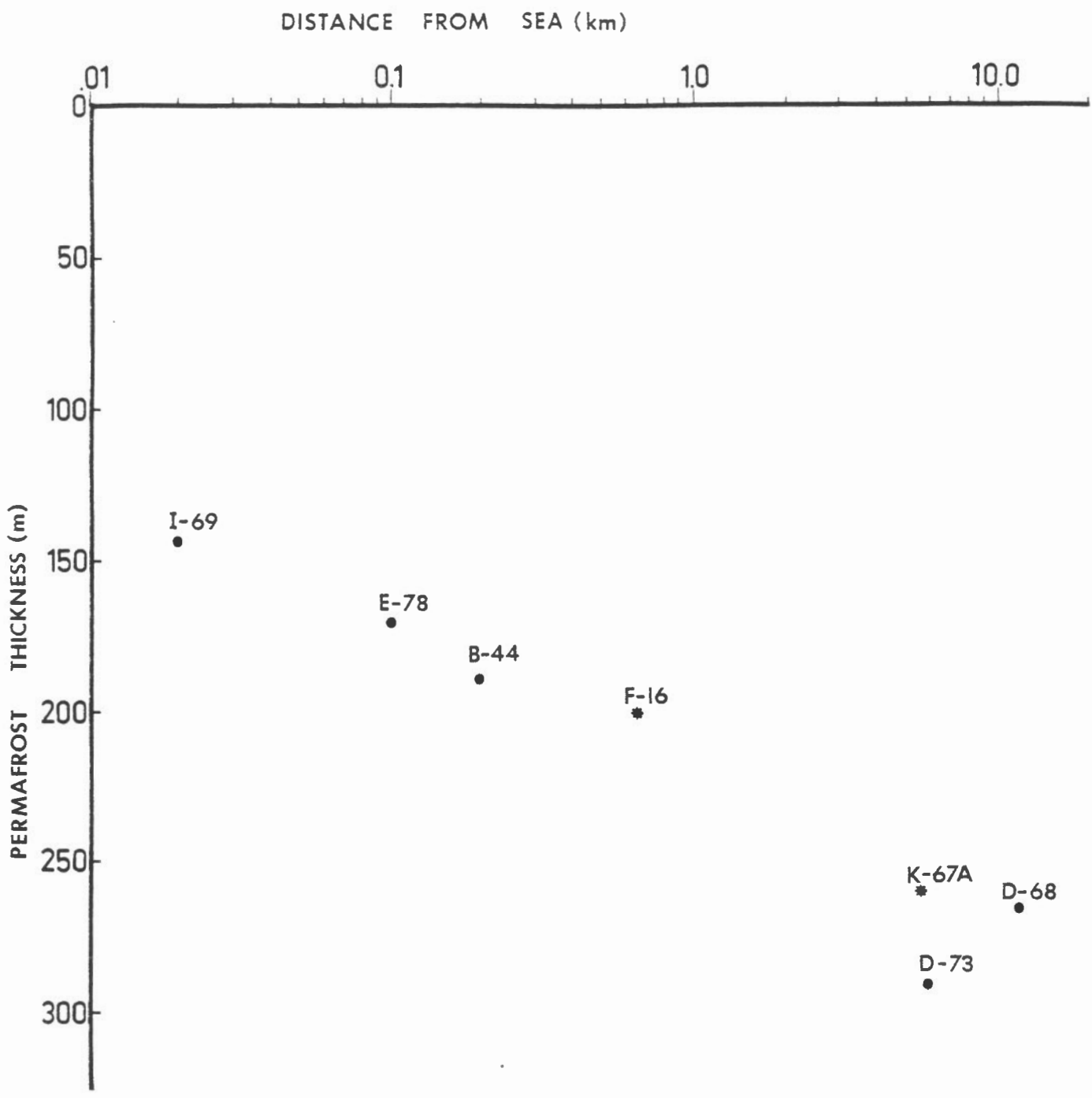

Figure 2. Permafrost thickness versus site distance from the present sea, Sabine Peninsula, Melville Island.

* = Assumed values.

Wellsites	Surficial Deposits	Vegetation Cover	Locality with Respect to Marine Limit	Periglacial Processes
Drake B-44	undifferentiated beach deposits underlain by Christopher shales and silts	>60% wet tundra meadows	b.m.l.	slumping and gullying along minor streams; tundra ponds
Drake E-78	veneer of undifferentiated colluvial deposits underlain by Christopher shales and silts	>60% saxifrage barrens	b.m.l.	slight gullying along streams
Drake D-73	undifferentiated alluvial deposits with some colluvial deposits underlain by Christopher shales and silts	>60% saxifrage barrens	b.m.l.	major slumping near sumps
Drake D-68	undifferentiated glaciofluvial deposits underlain by Christopher shales and silts	60% saxifrage barrens	b.m.l.	terrain disturbance; slumping of the sump; erosion and gullying along terrace and streams; ice wedges
Drake K-67A	undifferentiated glaciofluvial deposits underlain by Christopher shales and silts	60% saxifrage barrens	b.m.l.	terrain disturbance; modified by erosion and gullying
Drake F-16	undifferentiated shale deposits underlain by Christopher shales and silts	>60%	b.m.l.	modified by erosion and gullying
Hecla I-69	undifferentiated beach deposits underlain by Christopher shales and silts	60-75% moss & grass meadows	b.m.l.	terrain disturbance; coastal erosion; tundra ponds

Table 2. Characteristics for each wellsite.

2.

REGIONAL BACKGROUND

The Sabine Peninsula is located in the northeastern part of Melville Island, Northwest Territories (Figure 1). The island covers an area of approximately 42,476 km² and consists of lowlands, ridges, and plateaux underlain by rock of upper Paleozoic to early Tertiary Age (Tozer & Thorsteinsson, 1964).

2.1 Climate

Climatic data for Rea Point, shown in Figures 3 and 4, are the most representative of conditions on the Sabine Peninsula. However, the presence of large bodies of water (i.e. Byam Martin Channel; Hecla and Griper Bay) tend to reduce summer temperatures and increase the humidity on the Sabine Peninsula. Also, Rea Point is influenced significantly by the land mass of southeastern Melville Island.

Mean annual air temperature for Rea Point is -17.4°C and probably nearer to -18°C on the Sabine Peninsula (EBA Engineering Consultants Ltd., 1979; Maxwell, 1980). Strong temperature contrasts between land and sea may result from pack ice (in the winter and summer months), open water,

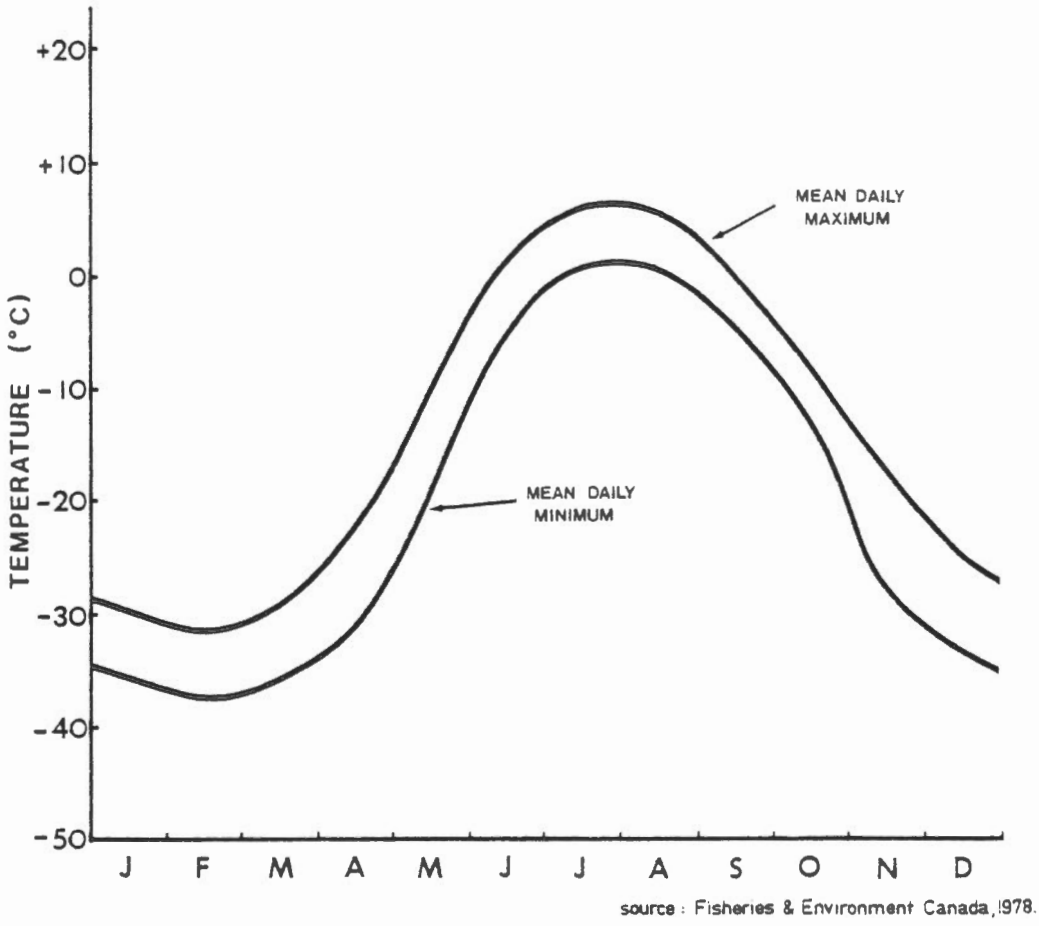

Figure 3. Temperature data for Rea Point, Melville Island.

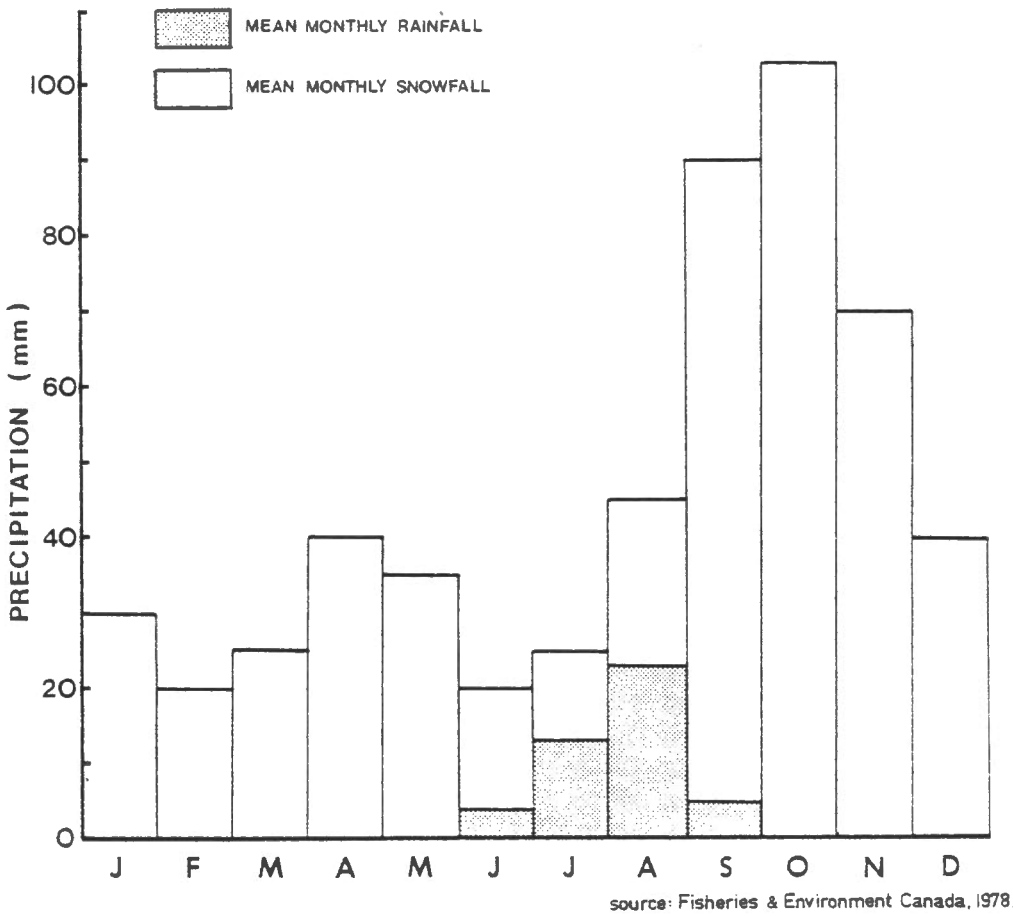

Figure 4. Precipitation data for Rea Point, Melville Island.

local terrain, or combinations of the three. Average wind speeds in the range of 18 kph to 22 kph have been recorded at Rea Point and similar speeds probably occur on the Sabine Peninsula. Snow accumulations are minimal and usually collect in depressions leaving much of the surface free of snow. Mean monthly rainfall at Rea Point is 20 mm in a time span of 4 months (Fisheries and Environment Canada, 1978). Snow cover, as well as rainfall, may vary between the Sabine Peninsula and Rea Point in response to local conditions.

Current knowledge indicates that the Sabine Peninsula is underlain by continuous permafrost with thicknesses ranging from 143 m to 288 m (Taylor et al., 1982).

2.2 Geology

The Sabine Peninsula lies near the axis of the Sverdrup Basin, a structural depression containing a thick (13,000 m) sequence of marine and nonmarine sedimentary rocks consisting mainly of sandstones and shales of lower and upper Cretaceous Age (see Figure 1) (Tozer and Thorsteinsson, 1964; Barnett et al., 1975; Balkwill, 1978). These are predominantly horizontal or gently dipping. They are overlain by a weathered and unconsolidated mantle of surficial materials (till, rubble, marine clay, sand and gravel) usually less than 2 m in thickness.

Four formations outcrop extensively on the Sabine Peninsula. The Christopher Formation, between 250-350 m thick, includes a basal member composed of shale, siltstone and sandstone with yellow calcareous concretions, a middle member composed of shale with yellow concretions, and an upper member composed of shale with some interbedded sandstone and dark red ironstone concretions (Tozer and Thorsteinsson, 1964). The Hassel Formation refers to red/brown nonmarine sandstone occurring stratigraphically between the Christopher and Kanguk shales. The approximate thickness of the Hassel Formation is 75 m. The Kanguk Formation lies stratigraphically above the Hassel Formation. A lower member is composed of fissile, light to dark grey shales, and an upper member is composed of light grey shales to dark red ironstone (Tozer and Thorsteinsson, 1964). The approximate thickness of the Kanguk Formation is 150 m. The Eureka Sound Formation, outcropping in the north of the peninsula, consists mainly of nonmarine yellow to white quartz sands with an approximate thickness of 90 m to 120 m.

Two circular piercement domes (Cape Colquhoun and Barrow domes) are composed of Pennsylvanian Age gypsum, limestone and gabbroic intrusive rock. These intrusions were emplaced as a result of the Eurekan orogeny (Thorsteinsson and Tozer, 1970).

Two formations appear at depth beneath the Sabine Peninsula. The Isachsen Formation consists mainly of light sandstone and conglomerate with some shale and extends

100 m to 1400 m below the Christopher Formation (Tozer and Thorsteinsson, 1964). The other is the Mould Bay Formation which comprises calcareous sandstone and claystone, and reaches a thickness of greater than 60 m.

2.3 Terrain

Major areas of the peninsula are underlain by soft shale of the Christopher Formation. These areas are identified by low undulating plains mantled with silty, clayey residual/colluvial soils. They are dissected by intricate networks of small ephemeral streams and braided channels. By contrast, the sandstone and shale of the Hassel and Kanguk Formations respectively produce distinct scarps and cuestas. The two circular piercement domes rise approximately 215 m above the undulating topography. In general, the elevations on the peninsula are low, averaging less than 75 m a.s.l. in the north to 150 m a.s.l. in the interior.

Periglacial processes on the peninsula include mass wasting, especially slopewash, solifluction, and rapid earthflows, together with a wide range of fluvial activities. Ground ice has been encountered in a number of shallow boreholes (EBA Engineering Consultants Ltd., 1979). On terrain underlain by either Christopher or Kanguk shales gullying and frequent thaw-flow slides occur. In general, much of the terrain of the Sabine Peninsula is considered highly sensitive to disturbance.

2.4 Late Quaternary History

Isostatic recovery, marine submergence, and Holocene coastal emergence all suggest that ice may have been present, either on, or adjacent to the Sabine Peninsula during late-Wisconsin times (McLaren and Barnett, 1978). The possibility of Pleistocene ice sheets has been discussed by Craig and Fyles (1960), Tozer and Thorsteinsson (1964), Fyles (1965), Blake (1970), England (1976a, b), Sugden (1977), Patterson (1977) and others. However, although a moraine system has been identified on the south coast of Melville Island (the Winter Harbour moraine), there is a general absence of fresh glacial landforms. In addition, stratigraphical evidence is not clear. As a result, the late Quaternary history of Eastern Melville Island is still obscure (McLaren and Barnett, 1978).

The existence of a late-Wisconsin, Innuitian Ice Sheet, rather than the Laurentide Ice Sheet, over the Western Queen Elizabeth Islands is suggested by varying patterns of early Holocene emergence. A high arctic ice cap (Innuitian Ice Sheet) originating in central Ellesmere Island and extending to eastern Bathurst Island is thought to be the most likely pattern of glaciation (Blake, 1970). This has been questioned by England (1976a, b), and England and Bradley (1978) who believe that Blake's (1970) Innuitian complex probably resulted from an extended section of the Greenland Ice Sheet.

Blake (1972) suggests that an ice lobe from the Laurentide Ice Sheet may have entered the channels between eastern Melville Island and Bathurst Island, and caused coastal depression. England (1976a, b) prefers a Franklin Ice Complex and takes greater consideration of the varying rates of emergence along the eastern and southern coasts of Melville Island.

The emergence curves on Figure 5 imply that ice thicknesses were greater in the vicinity of northeastern Melville Island than southern Melville Island. From the east and south coast curves, McLaren and Barnett (1978) indicate that the Sabine Peninsula is still recovering from post-glacial rebound at a rate of approximately 0.35 cm/yr. The curves offer two main possibilities: 1) deglaciation of southern Melville Island occurred previous to northeastern Melville Island, or 2) the increasing thickness of ice in the northeast provided greater glacio-isostatic loading in northeastern Melville Island than southern Melville Island (McLaren and Barnett, 1978).

Periods of submergence and emergence during late Quaternary and Holocene times resulted in a maximum marine limit on the Sabine Peninsula of approximately 60 m a.s.l. (Henoch, 1964; McLaren and Barnett, 1978). The inferred extent of post-glacial marine submergence is indicated in Figure 6. Barnett et al. (1977) report greater occurrences of slope instability, and higher moisture contents of sediments occurring below marine limit than above marine limit.

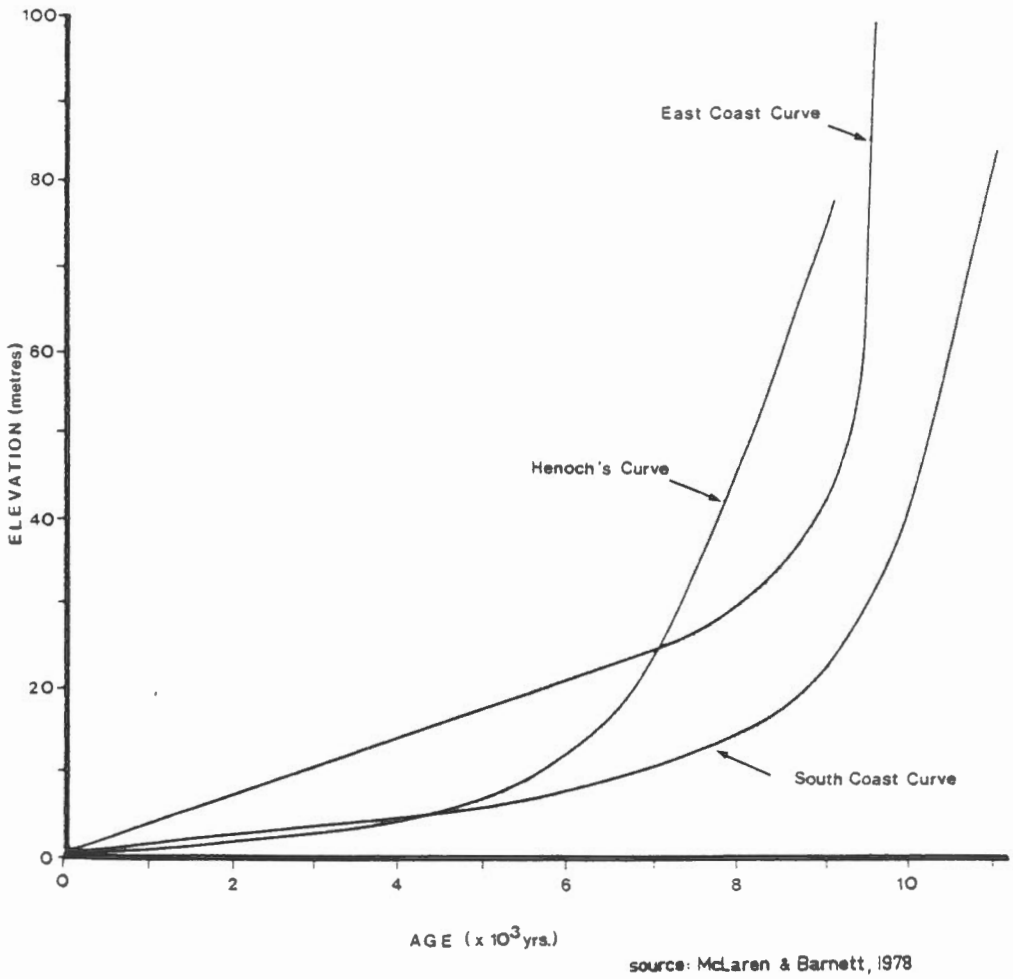

Figure 5. Comparison of emergence curves for Melville Island.

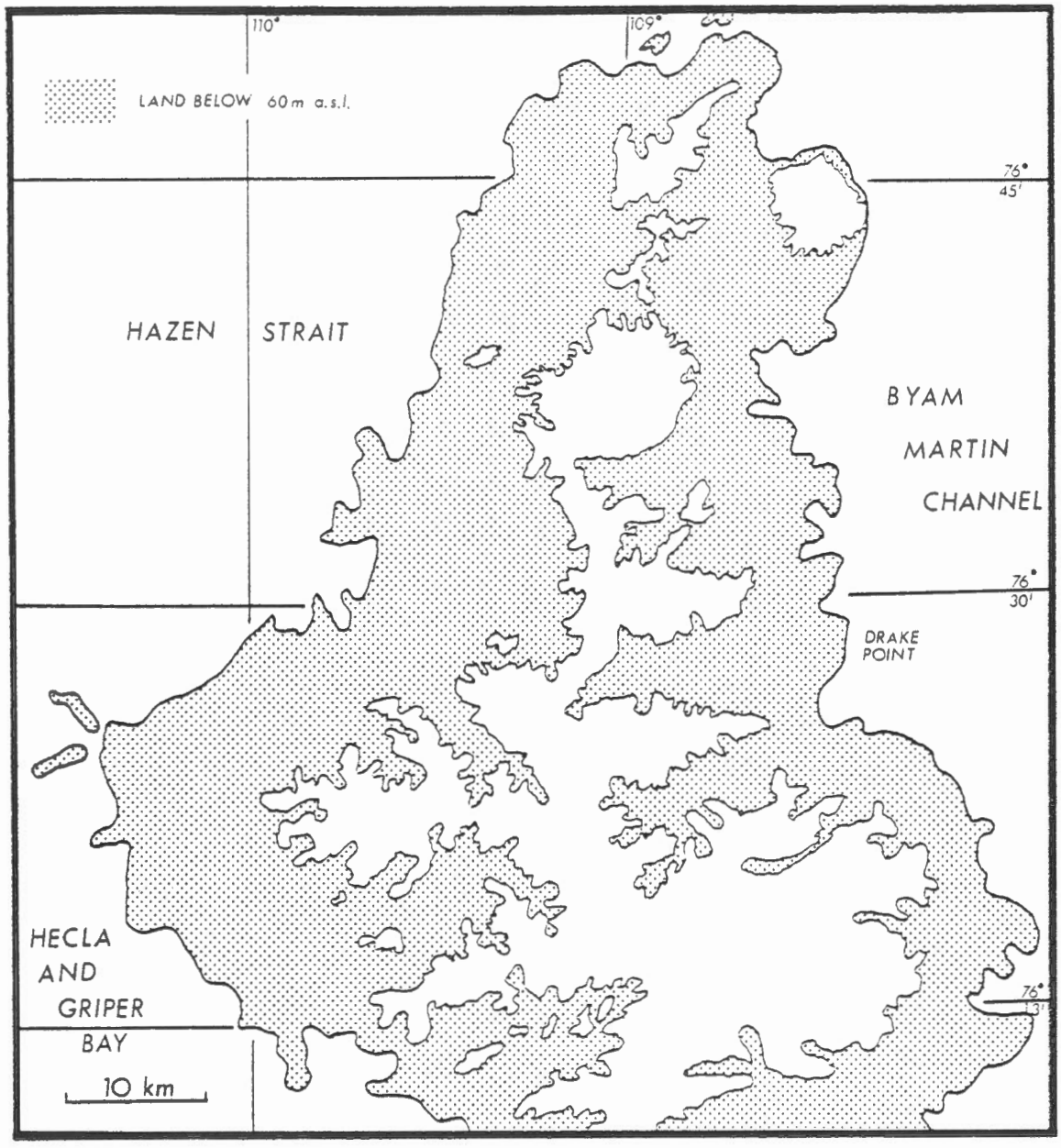

Figure 6. Approximate marine limit (60 m a.s.l.) on Sabine Peninsula, Melville Island.

3.

METHODOLOGY

3.1 Divided-Bar Apparatus

Thermal conductivities of crushed samples from drill cuttings were measured using the steady state divided-bar method (Figure 7). The divided-bar was of the type described by Judge (1973a; 1974a) (Figure 8). This method permits high accuracy measurements while using small temperature gradients across the sample. Accuracies of the method are approximately ±2% of the measured values.

Two cylindrical brass reservoirs were kept at different but constant temperatures by two refrigerated baths circulating water to the reservoirs. The cold bath was maintained at a temperature 5°C cooler than room temperature and the warm bath at a temperature 5°C warmer than room temperature. The warmer reservoir was placed above the sample to reduce the possibility of convective fluid movement in the porous samples. Between the reservoirs three discs, consisting of perspex, brass, and fused silica, were fastened together within a thin film of epoxy.

The perspex discs decrease the fluctuations of reservoir temperatures whereas the brass discs, having holes drilled radially in them, allow the insertion of

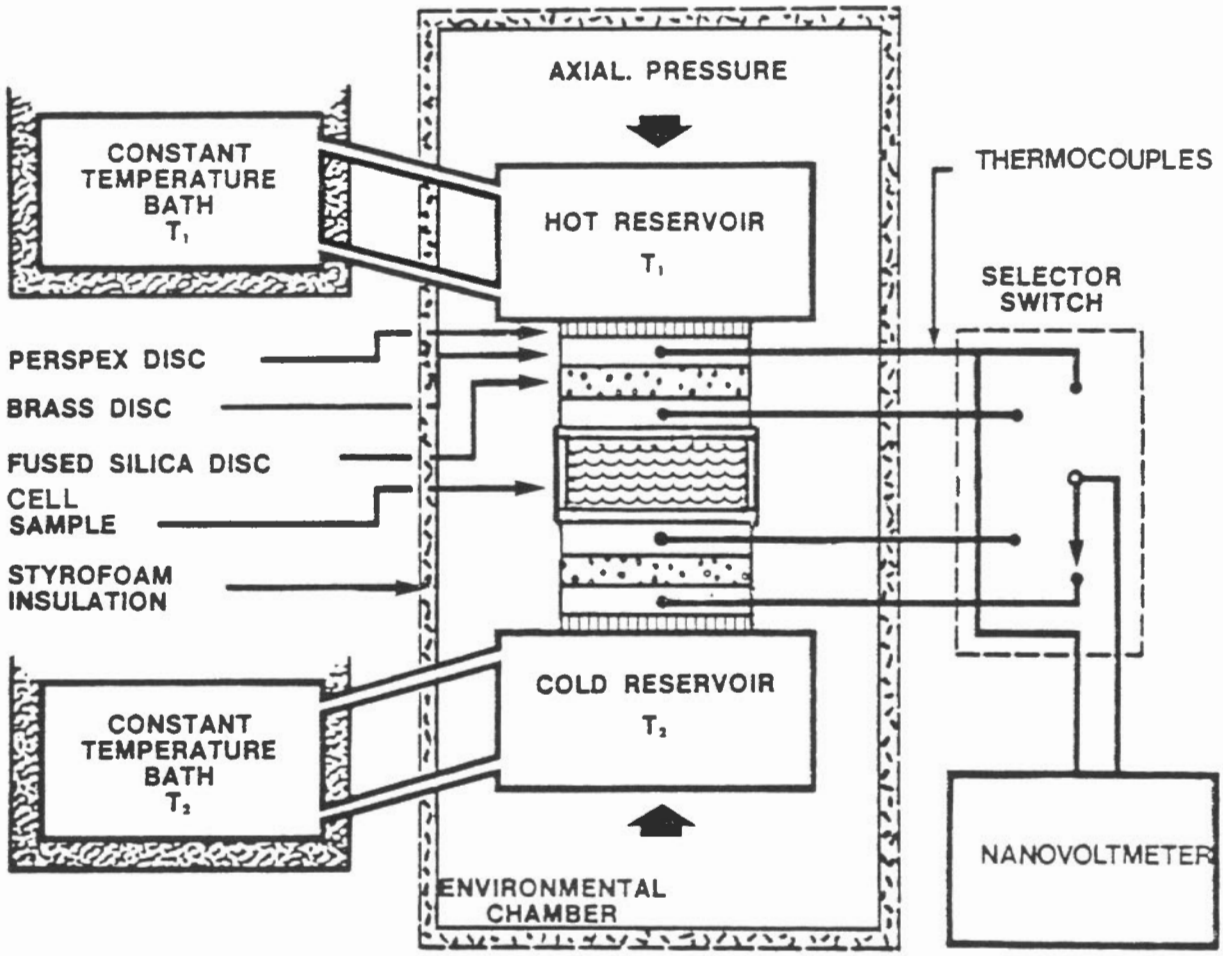

Figure 7. Diagrammatic illustration of divided-bar apparatus.

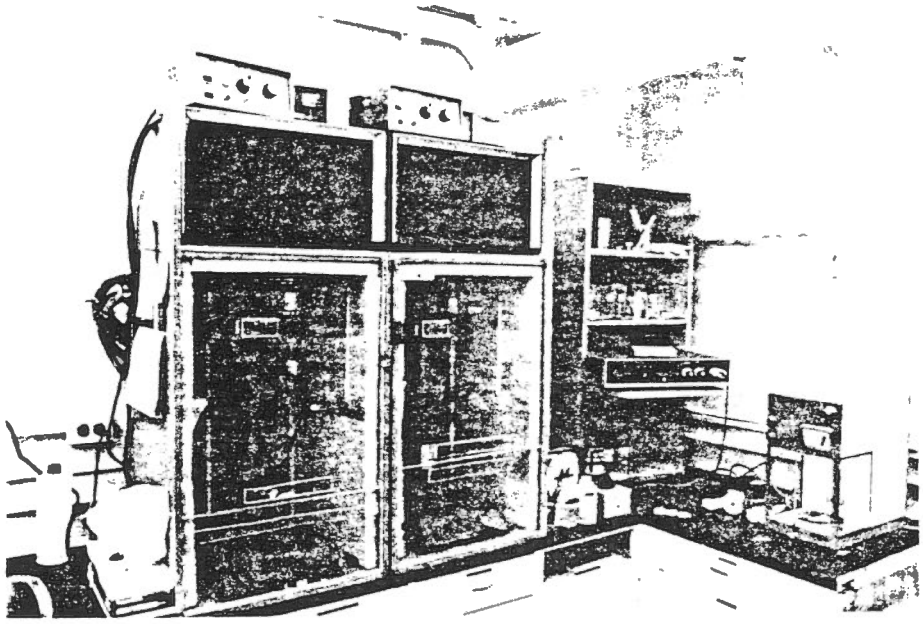

Figure 8. Laboratory facilities of Earth Physics Branch. Shown are two NESLAB RTE-4 type refrigerated baths (cold at top left; warm at top right) supplying water to reservoirs on two divided-bars situated in respective chambers. A Keithley 180 Digital Nanovoltmeter (located on shelves), a selector switch box (next to water bottles), and a Mettler H8 Balance (on black counter) compliment the required equipment. Three quartz standards are shown next to the selector switch box.

thermocouple sensors. The fused silica discs act as material of known thermal conductivity value (standards) in the divided-bar, a relative method. The temperature gradient across the discs of known value were compared to the temperature gradient across the sample to determine the unknown thermal conductivity of the sample. Four micro-miniature thermocouples of type TGC-1S-200 were used to measure the difference in EMF between a common junction and the discs in the bar, proportional to the temperature difference between the thermocouples. The entire divided-bar assembly is mounted in a hydraulic jack to allow axial pressures to be maintained on the cell sample, and thus reduce the contact resistance between the stack of discs, and the cell sample (Judge, 1974a). This assembly was placed inside an insulated box to ensure a constant temperature within the environmental chamber (Figure 9). After the cell sample was inserted between the two stacks, the apparatus was left for 10-15 minutes to allow the temperature to attain a steady state. Then, the temperature differences across the known conductivity of the fused silica discs and the unknown conductivity of the cell sample were measured using a Keithley 180 Digital Nanovoltmeter.

The fused and crystalline quartz standards and the values of the thermal conductivities of the materials established by Ratcliffe (1959) were used. Five standard fused silica (GE 101) discs of varying thicknesses (2.50, 5.00, 7.50, 10.00, and 12.50 cm) were placed between the

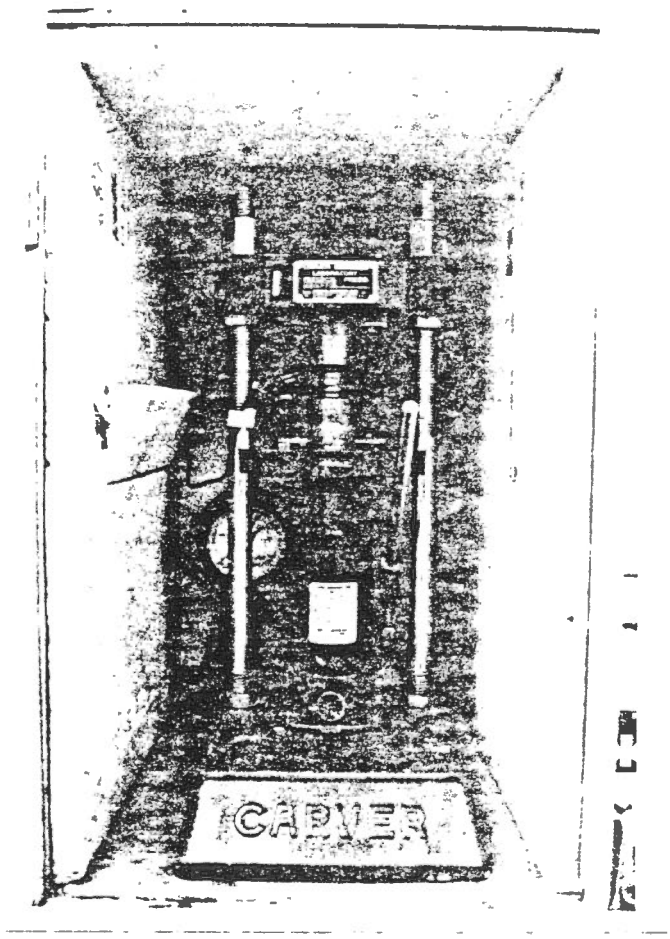

Figure 9. Divided-bar assembly with hydraulic jack inside insulated environmental chamber. Cell sample XX is shown between the stack of discs.

stacks to calibrate the bar in order to determine the temperature gradient across both the silica discs and the stack. After obtaining this gradient, the standard allowed the determination of the thermal conductivity of the intermediate fused silica disc (Judge, 1974a). Various problems and errors dealing with the design and use of the divided-bar apparatus are outlined by Jessop (1970).

Three measurements were made for every sample taken at approximately 30 m intervals. Samples were obtained by the rotary system technique (fluid circulation) whereby cuttings are brought up to the surface along the walls of the borehole. This procedure results in intermixing of drill cuttings from various lithologies during the drilling process. Drill cuttings were then randomly sampled from a "Shale Shaker" located near the drilling platform. The lithologies within the seven wells ranged from shale to sandstone.

3.2 Preparation of Cell Samples

Sixty-eight samples of drill cuttings from five boreholes (Drake E-78, Drake D-73, Drake D-68, Drake K-67A, and Drake F-16) were pulverized into grain size material and packed uniformly into cells. The latter consist of two brass discs of equal outer (3.185 cm) and inner (2.855 cm) diameter and thickness (2.360 cm), and a plastic ring (1,000 cm long) glued with epoxy on the bottom brass

disc (Figure 10). Cells were prepared by saturating crushed rock fragments with water containing a small amount of detergent. The presence of detergent prevents sample contamination from inherent substances and/or material within the cell. The packing procedure minimizes water content and eliminates air pockets. Distorted values may result from poorly packed cells containing air, since air has a very low thermal conductivity, approximately 0.024 $Wm^{-1}K^{-1}$. The cells were then placed in a vacuum oven (Figure 11) for approximately 12 to 14 hours to extract any existing air pockets within the sample. A glycerol/water solution was then applied to the top and bottom of the cell to provide a better contact with the stacks on both the hot and cold reservoirs.

Conductivity of the cell was determined in the same manner as if the cell were a disc of solid rock (Sass et al., 1971). A strip of parafilm was stretched around the plastic rim overlapping the lid to prevent either evaporation or sublimation of moisture. Once the measurement had been made, the top and bottom surfaces were wiped clean of the glycerol/water solution and the parafilm removed.

Different measurements on the cells prior to and after measuring the thermal conductivity of samples were taken. For example, after constructing the cells, the following were measured:

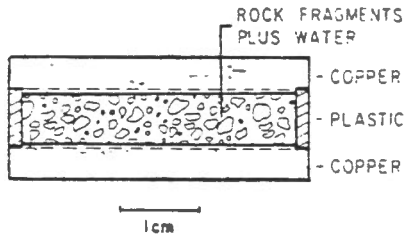

Figure 10. Scale diagram of the thermal conductivity cell (side view).

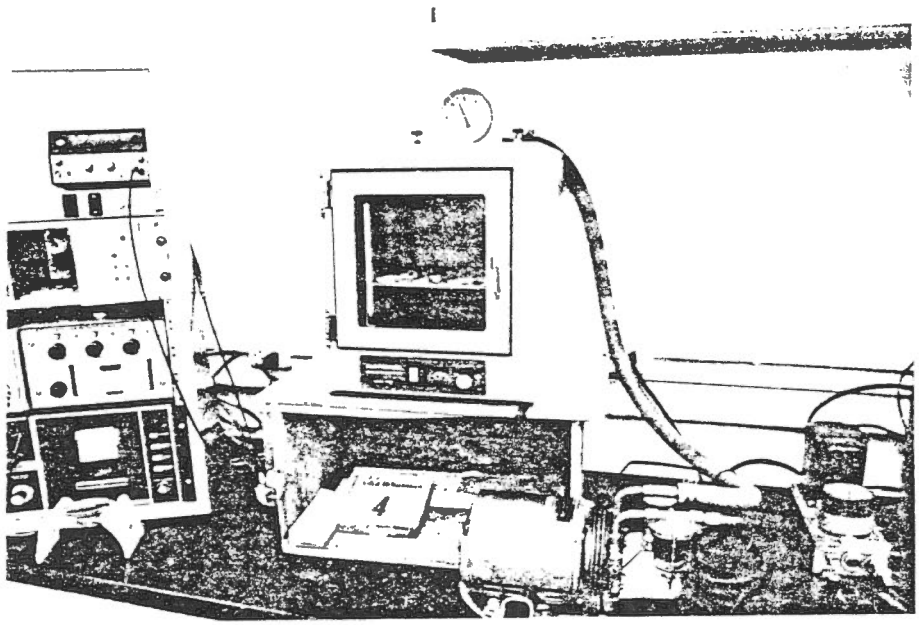

Figure 11. Vacuum oven with connecting pressure pump. Used for extraction of air pockets within cell samples.

1. the total thickness of the cell;
2. the thickness of the outer brass disc;
3. the sample thickness;
4. the outer and inner diameters of the plastic ring;
5. the cell weight.

Immediately following the thermal conductivity measurement, the wet sample weight was calculated by subtracting the cell weight from the wet weight and left to dry in order to determine the dry sample weight.

3.3 Analysis of Thermal Conductivities

The mean conductivity of the sample within the cell is inferred by the "Geometric" model mentioned in Judge (1974a) and Taylor (1978). This model was used to calculate in situ conductivities from measurements obtained from drill cuttings.

Since enclosing cell materials impose their own thermal conditions, problems in the calculation of the thermal conductivity values are encountered. These problems are eliminated by using the "Geometric" model to calculate the bulk conductivity of samples. The bulk thermal conductivity of the cell mixture within a cell was estimated by:

$$k_B = k_w^{\phi} k_g^{(1-\phi)} \qquad [1]$$

where k_B is the bulk thermal conductivity of the cell mixture;

k_w is the thermal conductivity of water ($0.55\ Wm^{-1}K^{-1}$);

k_g is the thermal conductivity of the grains in matrix;

ϕ is the porosity, volume fraction.

A computer program was used to correct the measured values since the conductivity of the entire cell (i.e. the two brass discs, the plastic ring, and the epoxy glue) is considered when the conductivity of the sample is determined. When this correction factor is considered, it is possible to obtain a thermal conductivity for the grains within the cell and then determine an estimated in situ thermal conductivity value with an assumed porosity from the following:

$$k_{is} = k_w^{\theta} k_g^{(1-\theta)} \qquad [2]$$

where k_{is} is the estimated in situ thermal conductivity;

k_w is the thermal conductivity of water ($0.55\ Wm^{-1}K^{-1}$);

k_g is the thermal conductivity of the grains (obtained from equation [1]);

θ is the assumed porosity of the formation (15-20%).

In situ thermal conductivities can be obtained for permafrost sections by substituting the thermal conductivity of water for the thermal conductivity of ice. Estimates of frozen and unfrozen *in situ* thermal conductivities were examined using equation [2]. It was noticed that thermal conductivities from estimated frozen *in situ* were higher than those estimated from unfrozen *in situ*. This may be explained by the fact that the thermal conductivity of water and ice are approximately 0.55 $Wm^{-1}K^{-1}$ and 2.22 $Wm^{-1}K^{-1}$, respectively (Clark, 1966). Judge (1973b, 1974a) showed that a rock with 10% porosity will possess a 14% higher thermal conductivity when ice-filled (frozen) rather than water-filled (unfrozen). Such was the case when assuming porosities of 15 and 20% for frozen and unfrozen *in situ* conductivities (Table 3). The determination of porosities for a number of samples of sandstones and shales from boreholes in the arctic by King (1977; 1979) led to the assumption of similar porosity values (15 to 20%) for each measured sample of the Sabine Peninsula. True porosities for the frozen and unfrozen sections of the wells can be determined from company well logs, but an assumed porosity value was thought appropriate for the present work. Table 3 lists the estimated *in situ* thermal conductivities for each geological formation.

Wellsites	Estimated Thermal Conductivities ($Wm^{-1}K^{-1}$) from Assumed Porosities (%) Water 15	Water 20	Ice 15	Ice 20	Depth (m)	Formation	Lithology
Drake B-44	2.9	2.6	3.6	3.5	30.0-140.0	Christopher	claystone
	2.8	2.5	3.4	3.3	140.0-390.0		shale
Drake E-78	2.1	1.9	2.5	2.5	30.5-121.9	Christopher	shale
	2.2	2.1	2.7	2.7	121.9-300.2		claystone
Drake D-73	2.3	2.1	2.1	2.8	30.5-396.0	Christopher	shale
Drake D-68	2.0	1.9	2.5	2.5	30.5-381.0	Christopher	shale
	2.3	2.2	2.9	2.9	381.0-518.2		sandstone
	2.5	2.3	3.1	3.0	518.2-701.0	Isachsen?	claystone
	3.1	2.8	3.8	3.7	701.0-795.5	Mould Bay?	sandstone
Drake K-67A	2.4	2.2	3.0	3.0	42.7-195.1	Christopher	claystone
	2.7	2.5	3.4	3.3	195.1-451.1		sandstone
Drake F-16	2.0	1.9	2.5	2.4	33.5-217.9	Christopher	shale
	2.2	2.0	2.7	2.7	217.9-274.3		claystone
	2.6	2.4	3.2	3.0	274.3-397.8		sandstone
Hecla I-69	2.0	1.8	2.4	2.4	30.0-350.0	Christopher	shale
	2.2*	2.0*	2.7*	2.7*	350.0-465.0	Isachsen	shale, siltstone
	2.3	2.2	2.9	2.9	465.0-610.0	Mould Bay	shale, sandstone

*assumed values

Table 3. Estimated in situ thermal conductivity values for varying geological formations.

4.

RESULTS

4.1 Introduction

The average conductivities for the formations appear to be similar and consistent from one borehole to another, with an overall variation of less than 20%. For example, the estimated thermal conductivity of Christopher shale, with an assumed porosity of 15%, was 2.3 $Wm^{-1}K^{-1}$ at Drake D-73, 2.1 $Wm^{-1}K^{-1}$ at Drake E-78, and 2.0 $Wm^{-1}K^{-1}$ at Drake F-16, Hecla I-69, and Drake D-68.

The bulk thermal conductivity values, as well as the estimated in situ thermal conductivity values for each sample from the seven wells are listed in Appendix A. The grain porosities and water contents within the cell samples, along with assumed porosity values are also included with the conductivities. Mean thermal conductivity values obtained from the "Geometric" model range from 2.7±0.2 $Wm^{-1}K^{-1}$ to 3.8±0.5 $Wm^{-1}K^{-1}$ for the seven wellsites. Moderately high values may be the result of high porosities ranging from 55 to 65% for shales, 35 to 60% for claystones, and 20 to 50% for sandstones. In addition, poor packing of cells caused by swelling of clay particles and variations in lithology within the cells (i.e. interbedding of shales of low thermal

conductivity with sandstone of high thermal conductivity) must be considered. The estimated in situ thermal conductivity values with porosities of 15 to 20% (for water and ice) are less than those previously derived from the "Geometric" model. Thus, high porosities tend to increase conductivities above the measured values from the model.

Thermal conductivity values shown in Appendix B represent plotted thermal conductivities with assumed porosities of 15% for ice above the permafrost base, and 15% for water below the permafrost base. A lack of drill cuttings for Hecla I-69 led to the insertion of assumed thermal conductivity values in the bottom section of the Christopher Formation and the entire Isachsen Formation. Assumed thermal conductivity values were also used for Drake D-73 to reduce high heat flow at a specific depth.

4.2 Analysis of Heat Flow

Heat flow values were calculated by a computer program modified by Dr. A. M. Jessop of the Earth Physics Branch. The program incorporates topographic, moving shoreline (with or without the effect of post-glacial emergence), and climatic corrections. It also converts borehole temperatures into corrected values for the required climatic history (Cermak and Jessop, 1971).

Heat flows from five wellsites were calculated by the interval method and the thermal depth method (i.e. the

"Bullard" heat flow). The interval method computes the heat flow in sections where temperature measurements are available. The computer program combined the product of the least square gradient of required temperature data in the section with the mean of the thermal conductivities from the same section to obtain a heat flow per section. The thermal depth method explained by Cermak and Jessop (1971) was also used for heat flow calculations. This method combines temperature at depth corrected for past climates, thermal conductivity, and mean surface temperature. Heat flows were calculated for every 30 and 190 m at the four Drake Pt. sites, and for every 30 and 250 m at Hecla I-69. These depths were arbitrarily chosen in response to any possible underground temperatures reflecting recent climatic changes, as well as irregularities or anomalies within borehole measurements. The climatic models shown in Figure 12 were used in the thermal depth method and corresponding heat flows listed in Table 4.

Several corrections to the temperature and heat flow are necessary. These are presented in Appendix B. First, a topographic correction takes into consideration large water bodies and undulating relief in the vicinity of the wellsite. The correction required elevation a.s.l. of the wellsite, mean surface temperature, sea water average temperature (-1.5°C), and geothermal gradient (Jaeger, 1965). Secondly, a moving shoreline correction was considered. This is of particular importance since all wellsites are located

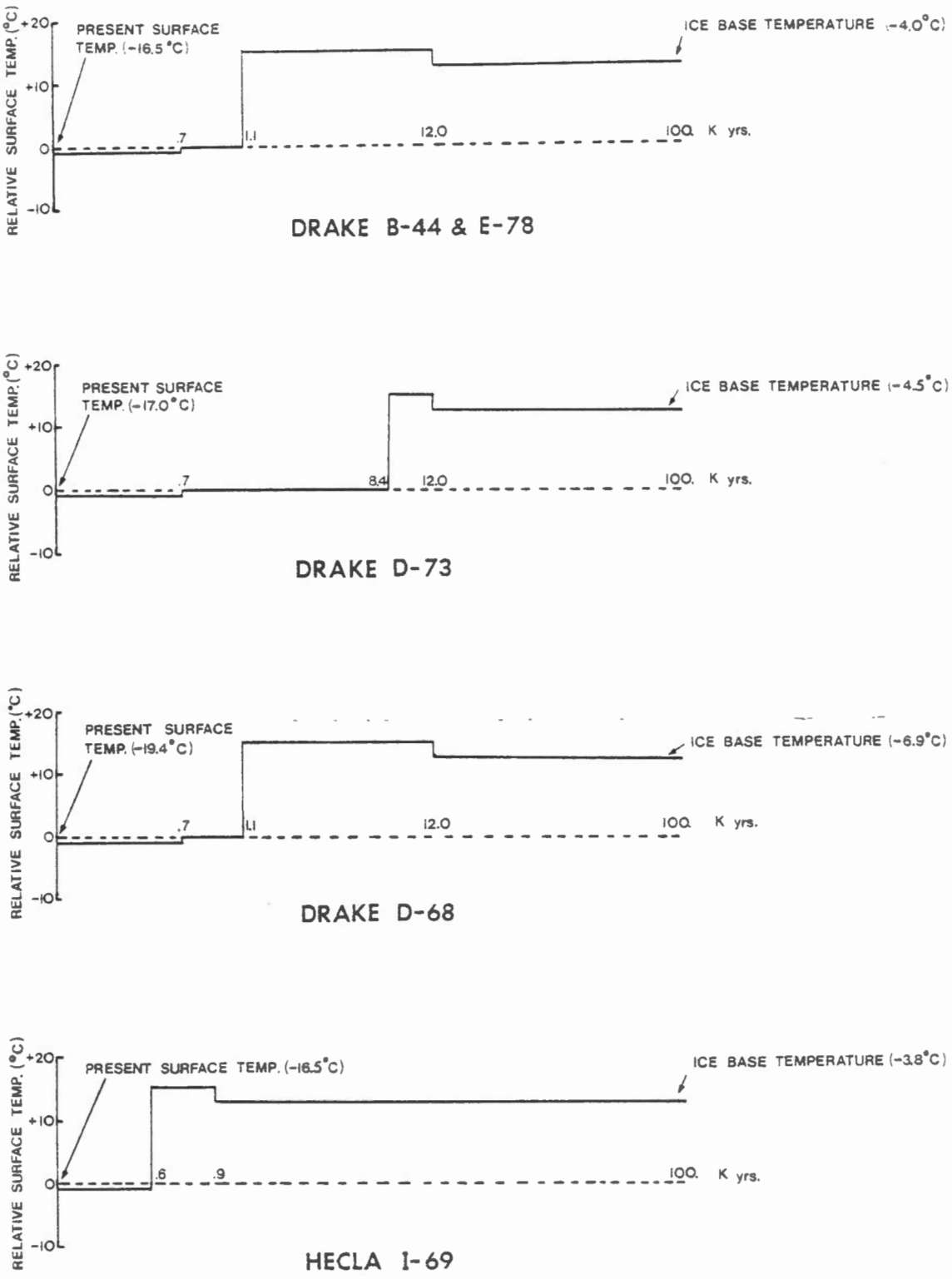

Figure 12. Models of past climate for the five wellsites.

Wellsites	Heat Flow (mWm^{-2}) Uncorrected	Corrected for Topography	Corrected for Moving Shorelines	Corrected for Climatic History
Drake B-44	108.0±3.7	117.7±3.9	67.1±2.2	63.1±2.2
Drake E-78	119.8±3.2	127.7±2.9	131.7±3.5	67.7±3.0
Drake D-68	107.1±3.3	106.3±3.3	80.6±1.9	76.8±2.7
Drake D-73	162.7±8.8	162.7±8.8	137.7±8.0	121.4±7.7[a]
	156.0±6.9	152.0±6.9	156.0±6.9	100.3±3.5[b]
Hecla I-69	77.9±2.9	80.9±2.5	80.4±3.2	72.4±2.0[c]
	73.9±2.4	76.7±2.0	76.3±2.6	69.9±2.2[d]

[a] without assuming any extra k values.
[b] assuming 5 extra k values.
[c] without assuming any extra k values.
[d] assuming 12 extra k values.

Table 4. Heat flow from Sabine Peninsula, Melville Island.

between .02 and 12.0 km from the shore. It is assumed that the mean surface (land) and sea water temperatures are different. Thirdly, a climatic correction was considered by using both an assumed climatic history of the area and an assumed ice-base temperature during glaciation. The theory and method of calculating climatic corrections to heat flow measurements are described by Birch (1948) and Crain (1969).

By introducing a correction for the effect of the last glaciation (Wisconsin) under the assumption that it terminated approximately 11,900 years ago (Denton and Hughes, 1981), one assumes surface temperatures relative to the present day. Climatic corrections are based on differences between the assumed temperatures in the past and extrapolated surface temperature from present observations. It is assumed that the prevailing temperature on the ice-ground boundary was close to pressure melting point during most of glacial times. A glacier base temperature of between -3.8 to -6.9°C was arbitrarily assumed. By using these values along with mean surface temperatures (Table 5), a difference of 13° was obtained. The four models shown in Figure 12 assume ice base temperatures and average surface temperatures of 1°C cooler than present for each wellsite. A probable error of 15 to 20% results from the climatic correction. Jessop (1968), and Cermak and Jessop (1971) report errors of 10 to 30% for similar corrections. Sharbatyan and Shumskiy (1974) identify problems when assuming a climatic correction.

Wellsites	Last Date Logged	Depth to 0° in m	Temperature Gradient in mKm^{-1}	Mean Surface Temperature in °C
Drake B-44	21.08.81	188	48	-16.5
Drake D-68	16.05.74	264	43	-19.4
Drake E-78	21.08.81	171	46	-16.5
Drake D-73	21.08.81	288	47	-17.0
Hecla I-69	12.05.80	143	43	-16.5
Drake K-67A	-	263*	-	-17.0*
Drake F-16	-	200*	-	-16.5*

* assumed values

Table 5. Measured permafrost thickness, temperature gradients, and mean surface temperatures for wellsites, Sabine Peninsula.

Table 4 lists the different heat flow values obtained by combining temperature gradients and thermal conductivities and applying various corrections. Corrected values ranged from 63 to 77 mWm^{-2} for the wellsites, with the exception of 115 mWm^{-2} for Drake D-73. Values for the Sabine Peninsula correspond to projected heat flows previously revealed by Judge (1973c; 1974b) and Judge and Jessop (1978) who expected the terrestrial heat flow to be high (50 to 84 mWm^{-2}) in the Sverdrup Basin because of evidence of igneous intrusions in Tertiary times.

According to Judge (1982, personal communication), the best indicator of terrestrial heat flow for the five wellsites on the Sabine Peninsula are heat flows below the permafrost base. The difference in heat flow above and below the permafrost base may explain permafrost aggradation at depth (Hunter et al., 1976). As shown in Appendix B, both uncorrected and corrected heat flows were also calculated by formation and lithology. Three wellsites revealed higher heat flows in the top formation than the adjacent formation. On the other hand, the low conductivity Christopher shales of Hecla I-69 and Drake D-68 reflected a lower heat flow than lower formations.

The measured heat flows obtained from the climatic correction become useful in determining permafrost thickness. Table 6 lists permafrost thicknesses that exceed actual values.

Wellsites	Permafrost Depth (m)				Ice Retreat
	Actual	Corrected for Topography	Corrected for Moving Shoreline	Corrected for Climatic History	$x10^3$ yrs. B.P.
Drake B-44	188	365	205	400	.6
Drake E-78	171	229	183	335	.5
Drake D-68	264	264	264	500	8.6
Drake D-73	288	285	281	413	8.4
Hecla I-69	143	365	153	657	.6

Table 6. Permafrost depths from various heat flow corrections for five wellsites.

5.

DISCUSSION AND CONCLUSIONS

Estimated porosities of 15 and 20% for ice and water resulted in lower in situ thermal conductivities than bulk thermal conductivities. Such porosities are in reasonable agreement with those obtained by King (1977; 1979) (e.g. 13% for shale; 17% for sandstones). The lower thermal conducitivity values reflect a high porosity (20%), whereas high thermal conductivity result from lower porosity (15%). The relative values for claystone and sandstone may be explained by the differences in shale content and porosity. Greater knowledge of porosities and conductivities at depth will reveal the actual sensitivity of measured values and involve more accurate assumptions when correcting for heat flows (i.e. climatic correction).

Lithological differences may account for the varying thermal conductivity values obtained from the seven wellsites. The thermal conductivity measurements cover a range of 2.0 to 4.8 $Wm^{-1}K^{-1}$. The values in Table 3 and Appendix A indicate similar agreement with other measured conductivities. For example, Judge (1973b) interpolates a thermal conductivity of approximately 2.8 $Wm^{-1}K^{-1}$ for shaley sandstone while Judge and Beck (1973) estimate a value of 2.4 $Wm^{-1}K^{-1}$ and Sass et al. (1971) report values ranging between 2.9 and

4.2 $Wm^{-1}K^{-1}$ for similar materials in different localities.

The mean of all heat flow values shown in Table 4 is 75.6±2.7 mWm^{-2}. Heat flow over the Sabine Peninsula appears to be relatively uniform from one site to another but dependent on distance from the sea. This may result from different temperature gradients and thermal conductivities for each formation, as well as present surface temperatures, influences of the present sea, and approximate times of ice retreat during the Pleistocene. The moderately high heat flows of the two inland sites (Drake D-68; Drake D-73) are partly attributed to undefined lithologies between the sampled drill cuttings, thermal disturbances caused by well completions (leading to temperature perturbations at depth), and influence of submergence of the area surrounding the wellsites.

Heat flow estimates for wells in the Sverdrup Basin range from 62.8 to 83.7 mWm^{-2}, 50.2 to 66.9 mWm^{-2} on the Parry Fold Belt, and 33.5 to 54.4 mWm^{-2} on the Arctic Platform (Judge, 1973b; 1974b). Therefore, the mean heat flow obtained for the Sabine Peninsula is well within the expected range for the Sverdrup Basin. The application of various corrections to the heat flow values reduce and change the heat flow curve. Climatic corrections assume Pleistocene ice base temperatures and average surface temperatures 1°C cooler than present. Heat flows obtained from the corrected model indicate permafrost thicknesses which could have existed in areas free of ice during late-Quaternary times.

The thickness of permafrost on the Sabine Peninsula decreases near the shoreline. Seismic velocity analyses in the area reveal similar thicknesses (Acheson, 1979; 1981). This decrease of permafrost near the shoreline may reflect submergence of the area by the sea prior to glacio-isostatic recovery. Since four sites are within one kilometre of the present shoreline, it might be appropriate to assume that permafrost thickness, thermal conductivity of the different lithologies within the wells, and site distance from the sea should vary proportionally with the time since emergence at each site (Taylor and Judge, 1981). McLaren and Barnett (1978) indicate that the Sabine Peninsula is still recovering from post-glacial rebound at a rate of approximately 0.35 cm/yr.

Present investigations indicate the need for both further field and laboratory studies directed toward thermal properties of materials, and subsurface thermal regimes. In addition, further studies on times of emergence, submergence, and ice sheet boundaries is of utmost importance in the complete understanding of this arctic environment.

6.

REFERENCES

Acheson, C. H. 1979. Estimate of permafrost thickness using seismic velocities. In, W. J. Scott and R. J. E. Brown, Ed., Proc. Symp. permafrost field methods and permafrost geophysics, October 3-4, 1977. N.R.C. Canada Tech. Mem. no. 124, Ottawa, pp. 101-124.

Acheson, C. H. 1981. Time-depth and velocity-depth relations in sedimentary basins--A study based on current investigation in the Arctic Islands and an interpretation of experience elsewhere. Geophysics, vol. 46, no. 5, pp. 707-716.

Balkwill, H. R. 1978. Evolution of Sverdrup Basin, Arctic Canada. Am. Assoc. Pet. Geol. Surv. Can., Paper 78-5, pp. 1004-1028.

Barnett, D. M., Edlund, S. A., and Dredge, L. A. 1977. Terrain characterization and evaluation: an example from eastern Melville Island. G.S.C. Paper 76-23.

Barnett, D. M., Edlund, S. A., Dredge, L. A., Thomas, D. C. and Prevett, L. S. 1975. Terrain classification and evaluation, eastern Melville Island. G.S.C., Open File No. 252.

Beck, A. E. 1957. Steady-state method for the rapid measurement of thermal conductivity of rocks. J. Sci. Instruments, 34, pp. 186-189.

Birch, F. 1948. The effect of Pleistocene climatic variations upon geothermal gradients. Am. J. Sci., 246, pp. 729-760.

Blake, W. 1970. Studies of glacial history in Arctic Canada. I. Pumice, radiocarbon dates, and differential postglacial uplift in the eastern Queen Elizabeth Islands. Can. J. Earth Sci., 7, pp. 634-664.

Blake, W. 1972. Climatic implications of radiocarbon-dated driftwood in the Queen Elizabeth Islands, Arctic Canada. In, Vasari, Y., Hyvärinen, H. and Hicks, S. (Eds.), Climatic changes in the Arctic during the last ten thousand years. A symposium held at Oulanka and Kevo, Finland, Oct. 1971, Acta Univ. Oulu, A3, Geol., 1, pp. 77-104.

Cermak, V., and Jessop, A. M. 1971. Heat flow generation and crustal temperature in the Kapuskasing area of the Canadian Shield. Tectonophysics, 11, pp. 287-303.

Clark, S. P. (Ed.) 1966. Handbook of physical constants, revised edition. Geological Society of America, Memoir 97, pp. 459-482.

Craig, B. G., and Fyles, J. G. 1960. Pleistocene geology of Arctic Canada. G.S.C., Paper 60-10.

Crain, I. K. 1969. A simple method of calculating climatic corrections to heat flow measurements. Can. J. Earth Sci., 6, pp. 499-502.

Denton, G. H., and Hughes, T. J. (Eds.) 1981. The last great ice sheets. John Wiley and Sons, Inc., 484 p.

EBA Engineering Consultants Ltd. 1979. Geotechnical Evaluation: Melville Island pipeline, Arctic Pilot Project. Submitted to the Alberta Gas Trunk Line Comp. Ltd., vol. 1-2.

England, J. H. 1976a. Postglacial isobases and uplift curves from the Canadian and Greenland High Arctic. Arctic and Alpine Research, 8, pp. 61-78.

England, J. H. 1976b. Late Quaternary glaciation of the eastern Queen Elizabeth Islands, Northwest Territories, Canada: alternative models. Quat. Res., 6, pp. 185-202.

England, J. H., and Bradley, R. S. 1978. Postglacial activity in the Canadian High Arctic. Science, 200, pp. 265-270.

Fisheries and Environment Canada 1978. An Arctic Atlas: Background information for developing marine oilspill countermeasures, August 1978. Arctic Marine Oilspill Rept., EPS-9-E-78-1, Environmental Impact Control Directorate.

Fyles, J. G. 1965. Surficial geology, western Queen Elizabeth Islands, G.S.C., Paper 65-1.

Henoch, W. E. S. 1964. Postglacial marine submergence and emergence of Melville Island, N.W.T. Geographical Bulletin, No. 22, pp. 105-126.

Hunter, J. A. M., Judge, A. S., MacAulay, H. A., Good, R. L., Gagné, R. M., and Burns, R. A. 1976. Permafrost and frozen sub-seabottom materials in the southern Beaufort Sea. Beaufort Sea Tech. Rep. No. 22, Beaufort Sea Proj., Department of the Environment.

Jaeger, J. C. 1965. Application of the theory of heat conduction to geothermal measurements. In Terrestrial heat flow, W. H. K. Lee (ed.). Geophysical Monograph Ser., 8, chapter 2.

Jessop, A. M. 1968. Three measurements of heat flow in Eastern Canada. Can. J. Earth Sci., 5, pp. 1-8.

Jessop, A. M. 1970. The effect of environment on divided-bar measurements. Tectonophysics: 10, pp. 39-49.

Judge, A. S. 1973a. The measurement of thermal conductivity of earth materials. In, Proceedings of a seminar on the thermal regime and measurements in permafrost 2 and 3 May 1972, prepared by R. J. E. Brown, Tech. Mem. No. 108, pp. 26-31.

Judge, A. S. 1973b. The prediction of permafrost thicknesses. Can. Geotech. J., 10, p. 1-11.

Judge, A. S. 1973c. Deep temperature observations in the Canadian North. Proc. Second Int. Permafrost Conf., Yakutsk, Nat. Acad. Sci. (U.S.A.), pp. 35-40.

Judge, A. S. 1974a. Thermal regime of the Mackenzie Valley: Observations of the Natural State Report. Environmental-Social Committee on Northern Pipelines, Report No. 73-38, 175 p.

Judge, A. S. 1974b. Geothermal measurements in northern Canada. Proc. Symp. Geology of the Canadian Arctic, GAC/CSPC, pp. 301-311.

Judge, A. S., and Beck, A. E. 1973. Analysis of heat-flow data--Several boreholes in a sedimentary basin. Can. J. Earth Sci., 10, pp. 1494-1507.

Judge, A. S., and Jessop, A. M. 1978. Heat flow north of 60° N. Arctic Geophysical Review. J. F. Sweeney (ed.). Publications of the Earth Physics Branch, vol. 45, no. 4, pp. 25-33.

King, M. S. 1977. Acoustic velocities and electrical properties of frozen sandstones and shales. Can. J. Earth Sci., 14, pp. 1004-1013.

King, M. S. 1979. Thermal conductivity measurements on saturated rocks at permafrost temperatures. Can. J. Earth Sci., 16, pp. 73-79.

Maxwell, J. B. 1980. The climate of the Canadian Arctic Islands and adjacent waters. Environment Canada, A.E.S., 531 p.

McLaren, P., and Barnett, D. M. 1978. Holocene emergence of the south and east coasts of Melville Island, Queen Elizabeth Islands, Northwest Territories, Canada. Arctic, vol. 31, No. 4, pp. 415-427.

Paterson, W. S. B. 1977. Extent of the late-Wisconsin glaciation in northwest Greenland and northern Ellesmere Island: a review of the glaciological and geological evidence. Quat. Res., 8, pp. 180-190.

Ratcliffe, E. H. 1959. Thermal conductivities of fused and crystalline quartz. Brit. J. Appl. Physics, 10, pp. 22-15.

Sass, J. H., Lachenbruch, A. H., and Munroe, R. J. 1971. Thermal conductivity of rocks from measurements on fragments and its application of heat flow determinations. J. Geophys. Res., 76, No. 14, pp. 3391-3401.

Sharbatyan, A. A., and Shumskiy, P. A. 1974. Extreme estimations in Geothermy and Geocryology. Translated by U.S. Joint Pub. Res. Serv. for CRREL, Draft Translation 465, 140 p.

Sugden, D. E. 1977. Reconstruction of the morphology, dynamics, and thermal characteristics of the Laurentide ice sheet at its maximum. Arctic and Alpine Research, vol. 9, no. 1, pp. 21-47.

Taylor, A. E. 1978. Temperatures and heat flow in a system of cylindrical symmetry including a phase boundary. Geothermal Series No. 7, Geothermal Service of Canada, Earth Physics Branch of Energy, Mines and Resources, Ottawa, 95 p.

Taylor, A. E. and Judge, A. S. 1975. Canadian geothermal data collection--Northern wells 1974. Geothermal Series Number 3, Earth Physics Branch, Energy, Mines and Resources, Ottawa, 127 p.

Taylor, A. E. and Judge, A. S. 1981. Measurement and prediction of permafrost thickness, Arctic Canada. Presented at 51st annual meeting, Society of Exploration Geophysicists, Los Angeles, Ca., October 1981, 15 p.

Taylor, A. E., Burgess, M., Judge, A. S., and Allen, V. S. 1982. Canadian geothermal data collection--northern wells 1981. Geothermal Series No. 13, Geothermal Service of Canada, Earth Physics Branch, Department of Energy, Mines and Resources, Ottawa, 153 p.

Thorsteinsson, R., and Tozer, E. T. 1970. Geology of the Arctic Archipelago. In, Douglas, R. J. W. (ed.), Geology and Economic Minerals of Canada. Geol. Surv. Can., Econ. Geol. Rep., No. 1, pp. 548-590.

Tozer, E. T., and Thorsteinsson, R. 1964. Western Queen Elizabeth Islands, Arctic Archipelago. G.S.C. Memoir 332, 242 p., incl. Map 1142A.

APPENDIX A

THERMAL CONDUCTIVITY MEASUREMENTS FOR SEVEN WELLSITES, SABINE PENINSULA

Depth (m)	Mean Grain Density Mgm^{-3}	Mean Water Content %	Mean Thermal Conductivity from Geometric Model $Wm^{-1}K^{-1}$	Estimated Mean in situ Thermal Conductivity ($\overline{Wm^{-1}K^{-1}}$) from Assumed Porosities (%) water .15	water .20	ice .15	ice .20	Lithology
30.5	2.50	59	2.7±0.5	2.1	2.0	2.6	2.6	Christopher Formation shale
60.9	2.53	60	2.8±0.3	2.2	2.0	2.7	2.6	shale
89.9	2.47	58	2.4±0.1	1.9	1.8	2.3	2.3	shale
121.9	2.51	58	2.8±0.3	2.2	2.0	2.7	2.7	claystone
155.4	2.52	62	2.9±0.7	2.2	2.0	2.7	2.7	claystone
182.9	2.52	56	2.8±0.4	2.2	2.0	2.7	2.7	claystone
213.4	2.51	58	2.8±0.5	2.2	2.0	2.7	2.6	claystone
245.4	2.50	54	2.8±0.2	2.3	2.0	2.7	2.7	claystone
281.9	2.50	55	3.0±0.3	2.3	2.1	2.9	2.8	claystone
300.2	2.58	59	2.8±0.1	2.2	2.0	2.7	2.7	claystone
Mean Values	2.51	58	2.8±0.3	2.2	2.0	2.7	2.6	

Table A-1. Thermal conductivity measurements derived from the geometric model and estimated in situ thermal conductivity values for Drake E-78, Sabine Peninsula.

Depth (m)	Mean Grain Density Mgm^{-3}	Mean Water Content %	Mean Thermal Conductivity from Geometric Model $Wm^{-1}K^{-1}$	Estimated Mean in situ Thermal Conductivity ($\overline{Wm^{-1}K^{-1}}$) from Assumed Porosities (%) water .15	water .20	ice .15	ice .20	Lithology
								Christopher Formation
30.5	2.61	60	2.6±0.4	2.1	1.9	2.6	2.5	shale
60.9	2.60	61	2.9±0.4	2.3	2.1	2.8	2.8	shale
91.4	2.58	58	2.9±0.3	2.3	2.1	2.8	2.8	shale
121.9	2.59	58	3.2±0.5	2.5	2.3	3.0	2.9	shale
152.4	2.56	56	3.3±0.4	2.5	2.3	3.1	3.0	shale
182.9	2.58	60	3.1±0.4	2.5	2.2	2.9	2.8	shale
213.4	2.64	60	3.1±0.4	2.4	2.2	2.9	2.9	shale
243.8	2.44	60	2.8±0.4	2.2	2.0	2.7	2.6	shale
274.3	2.51	62	3.0±0.5	2.3	2.1	2.9	2.8	shale
304.8	2.57	57	3.2±0.3	2.5	2.3	3.0	3.0	shale
335.3	2.51	57	2.9±0.2	2.3	2.1	2.8	2.8	shale
365.8	2.52	58	2.7±0.3	2.1	1.9	2.6	2.6	shale
396.2	2.55	58	2.4±0.1	1.9	1.8	2.4	2.4	shale
Mean Values	2.56	59	2.9±0.3	2.3	2.1	2.8	2.8	

Table A-2. Thermal conductivity measurements derived from the geometric model and estimated in situ thermal conductivity values for Drake D-73, Sabine Peninsula.

Depth (m)	Mean Grain Density Mgm^{-3}	Mean Water Content %	Mean Thermal Conductivity from Geometric Model $Wm^{-1}K^{-1}$	Estimated Mean in situ Thermal Conductivity ($\overline{Wm^{-1}K^{-1}}$) from Assumed Porosities (%) water .15	water .20	ice .15	ice .20	Lithology
								Christopher Formation
30.5	2.75	59	2.3±0.1	1.8	1.7	2.3	2.2	shale
60.9	2.70	57	2.3±0.1	1.9	1.8	2.3	2.3	shale
106.7	2.68	54	2.4±0.1	1.9	1.8	2.4	2.4	shale
152.4	2.71	58	2.4±0.2	1.9	1.8	2.4	2.4	shale
182.9	2.66	56	2.3±0.1	1.9	1.8	2.3	2.3	shale
228.6	2.67	50	2.8±0.1	2.2	2.0	2.7	2.6	shale
274.3	2.64	48	2.5±0.1	2.0	1.8	2.4	2.4	shale
304.8	2.67	47	2.7±0.1	2.2	2.0	2.6	2.6	shale
335.3	2.73	44	3.0±0.1	2.3	2.1	2.8	2.8	shale
381.0	2.72	50	2.8±0.1	2.2	2.0	2.7	2.7	shale
426.7	2.59	37	2.3±0.1	1.8	1.7	2.2	2.3	sandstone
457.2	2.69	33	3.1±0.2	2.4	2.2	2.9	2.9	claystone
484.6	2.67	32	4.1±0.3	3.0	2.7	3.7	3.6	sandstone
518.2	2.72	42	2.7±0.2	2.1	2.0	2.6	2.6	claystone
548.6	2.71	42	2.7±0.2	2.2	2.0	2.7	2.6	claystone
579.1	2.68	43	2.7±0.1	2.1	2.0	2.6	2.6	claystone
606.6	2.86	38	3.6±0.1	2.7	2.5	3.3	3.2	claystone
640.1	2.72	37	3.4±0.1	2.6	2.4	3.2	3.1	claystone
670.6	2.82	28	4.6±0.4	3.4	3.0	4.1	4.0	claystone
701.0	2.81	35	3.7±0.1	2.8	2.5	3.4	3.4	sandstone
731.5	2.67	23	4.3±0.4	3.2	2.9	3.9	3.8	sandstone
762.0	2.57	28	4.3±0.5	3.1	2.8	3.8	3.7	sandstone
795.5	2.66	29	4.4±0.7	3.2	2.9	4.0	3.9	sandstone
Mean Values	2.70	42	3.1±0.2	2.4	2.3	2.9	2.8	

Table A-3. Thermal conductivity measurements derived from the geometric model and estimated in situ thermal conductivity values for Drake D-68, Sabine Peninsula.

Depth (m)	Mean Grain Density Mgm^{-3}	Mean Water Content %	Mean Thermal Conductivity from Geometric Model $Wm^{-1}K^{-1}$	Estimated Mean in situ Thermal Conductivity ($\overline{Wm^{-1}K^{-1}}$) from Assumed Porosities (%) water .15	water .20	ice .15	ice .20	Lithology
								Christopher Formation
42.7	2.46	45	3.5±0.8	2.3	2.1	2.8	2.7	claystone
88.4	2.74	49	3.9±0.2	2.9	2.7	3.6	3.5	claystone
140.2	2.75	54	3.1±0.3	2.4	2.2	3.0	2.9	claystone
195.1	2.80	52	2.5±0.4	1.8	1.7	2.5	2.4	sandstone
246.9	2.85	40	3.3±0.1	2.6	2.3	3.1	3.1	sandstone
280.4	3.01	43	3.7±0.5	3.0	2.7	3.4	3.5	sandstone
301.8	2.81	51	3.3±0.5	2.5	2.3	3.1	3.0	claystone
329.2	2.82	37	4.3±0.4	3.2	2.9	3.9	3.8	sandstone
356.6	2.81	41	3.5±0.4	2.6	2.4	3.2	3.2	sandstone
393.2	2.84	39	3.4±0.1	2.6	2.4	3.2	3.1	sandstone
451.1	2.95	38	4.1±0.3	3.0	2.7	3.7	3.6	sandstone
Mean Values	2.80	44	3.5±0.4	2.6	2.4	3.2	3.2	

Table A-4. Thermal conductivity measurements derived from the geometric model and estimated in situ thermal conductivity values for Drake K-67A, Sabine Peninsula.

Depth (m)	Mean Grain Density Mgm^{-3}	Mean Water Content %	Mean Thermal Conductivity from Geometric Model $Wm^{-1}K^{-1}$	Estimated Mean in situ Thermal Conductivity ($\overline{Wm^{-1}K^{-1}}$) from Assumed Porosities (%) water .15	water .20	ice .15	ice .20	Lithology
								Christopher Formation
33.5	2.68	62	2.6±0.2	2.1	1.9	2.6	2.5	shale
67.1	2.59	63	2.4±0.2	1.9	1.8	2.3	2.3	shale
102.1	2.41	59	2.4±0.7	1.9	1.8	2.3	2.3	shale
118.9	2.61	65	2.6±0.5	2.0	1.9	2.5	2.5	shale
169.2	2.63	59	2.6±0.2	2.1	1.9	2.5	2.5	shale
217.9	2.67	57	2.6±0.1	2.1	1.9	2.6	2.5	claystone
251.5	2.71	48	2.6±0.5	2.3	2.1	2.9	2.8	claystone
274.3	2.82	41	3.2±0.2	2.5	2.3	3.0	3.0	sandstone
307.8	2.85	37	3.7±0.4	2.9	2.7	3.6	3.3	sandstone
397.8	2.67	47	3.0±0.3	2.3	2.1	2.8	2.8	sandstone
Mean Values	2.66	54	2.8±0.3	2.2	2.0	2.7	2.6	

Table A-5. Thermal conductivity measurements derived from the geometric model and estimated in situ thermal conductivity values for Drake F-16, Sabine Peninsula.

Depth (m)	Mean Grain Density Mgm^{-3}	Mean Thermal Conductivity from Geometric Model $Wm^{-1}K^{-1}$	Estimated Mean in situ Thermal Conductivity ($\overline{Wm^{-1}K^{-1}}$) from Assumed Porosities (%) water .15	water .20	ice .15	ice .20	Lithology
							Christopher Formation
30.5	2.64	3.9±0.5	2.9	2.7	3.6	3.5	claystone
64.0	2.63	4.1±0.5	3.1	2.8	3.8	3.6	claystone
88.4	2.65	5.4±0.7	3.9	3.4	4.8	4.5	claystone
112.8	2.66	2.9±0.4	2.3	2.1	2.8	2.8	claystone
134.1	2.63	3.3±0.5	2.5	2.3	3.1	3.0	claystone
152.4	2.74	4.8±0.6	3.5	3.1	4.3	4.1	shale
182.9	2.66	3.6±0.1	2.7	2.5	3.3	3.2	shale
204.2	2.58	3.7±0.8	2.8	2.5	3.4	3.3	shale
234.7	2.66	3.9±0.3	2.9	2.6	3.5	3.5	shale
271.3	2.73	3.5±0.2	2.7	2.4	3.3	3.2	shale
289.6	2.69	2.7±0.1	2.1	2.0	2.6	2.6	shale
301.7	2.59	3.4±0.6	2.6	2.4	3.2	3.1	shale
320.0	2.68	4.4±0.9	3.2	2.9	3.9	3.8	shale
335.3	2.71	3.6±0.3	2.7	2.5	3.4	3.3	shale
371.8	2.65	3.3±0.5	2.5	2.3	3.1	3.0	shale
Mean Values	2.66	3.8±0.5	2.8	2.6	3.5	3.4	

Table A-6. Thermal conductivity measurements derived from the geometric model and estimated in situ thermal conductivity values for Drake B-44, Sabine Peninsula.

Depth (m)	Mean Grain Density Mgm^{-3}	Mean Thermal Conductivity from Geometric Model $Wm^{-1}K^{-1}$	Estimated Mean in situ Thermal Conductivity ($\overline{Wm^{-1}K^{-1}}$) from Assumed Porosities (%) water .15	water .20	ice .15	ice .20	Lithology
							Christopher Formation
30.5	2.49	2.0±0.2	1.7	1.6	2.1	2.1	shale
64.0	2.37	2.4±0.1	1.9	1.8	2.4	2.3	shale
88.4	2.53	2.9±0.1	2.3	2.1	2.8	2.8	shale
121.9	2.46	2.5±0.1	2.0	1.8	2.4	2.4	shale
213.4	2.53	2.5±0.2	2.0	1.8	2.4	2.4	shale
							Isachsen Formation
457.2	2.60	3.4±0.3	2.6	2.3	3.2	3.1	shale, siltstone
							Mould Bay Formation
472.4	2.64	2.5±0.2	2.0	1.9	2.5	2.5	shale
487.7	2.63	2.5±0.1	2.0	1.9	2.5	2.5	shale
499.8	2.49	2.6±0.2	2.0	1.9	2.5	2.5	shale
521.2	2.54	2.9±0.2	2.2	2.1	2.8	2.7	shale
551.7	2.49	3.3±0.5	2.5	2.3	3.1	3.0	shale
560.8	2.50	2.9±0.5	2.3	2.1	2.9	2.8	shale
579.1	2.46	2.4±0.4	1.9	1.8	2.4	2.4	shale
594.4	2.53	2.7±0.2	2.2	2.0	2.7	2.6	shale
609.6	2.50	2.5±0.2	2.0	1.9	2.5	2.5	claystone
Mean Values	2.52	2.7±0.2	2.1	1.9	2.6	2.6	

Table A-7. Thermal conductivity measurements derived from the geometric model and estimated in situ thermal conductivity values for Hecla I-69, Sabine Peninsula.

APPENDIX B

HEAT FLOW PROFILES FOR FIVE WELLSITES, SABINE PENINSULA

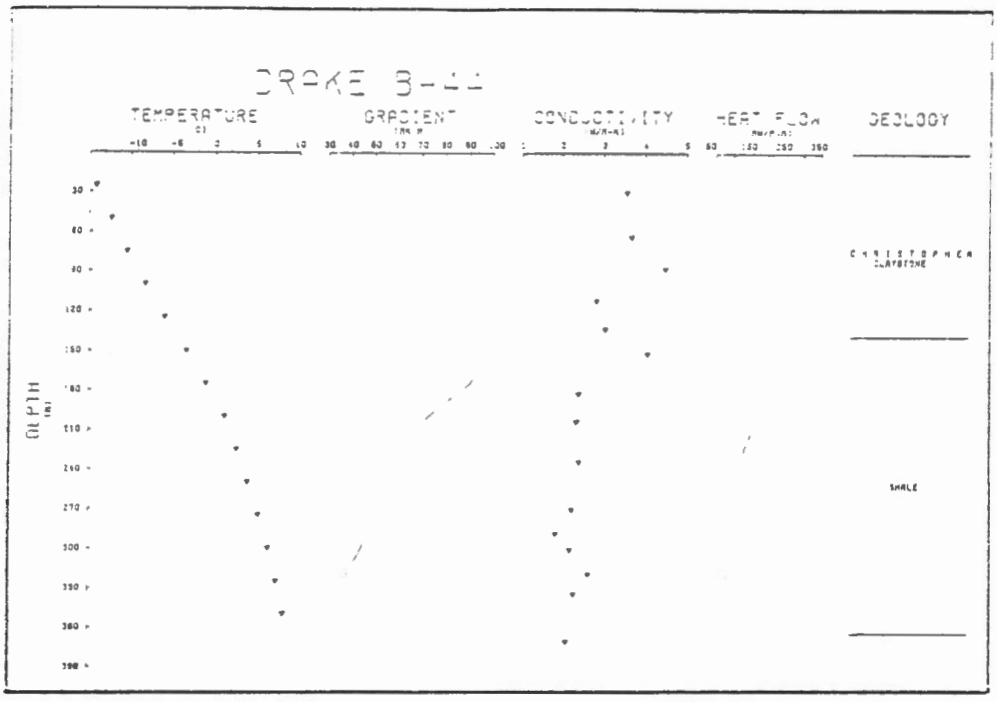

Figure B-1. Uncorrected heat flow.

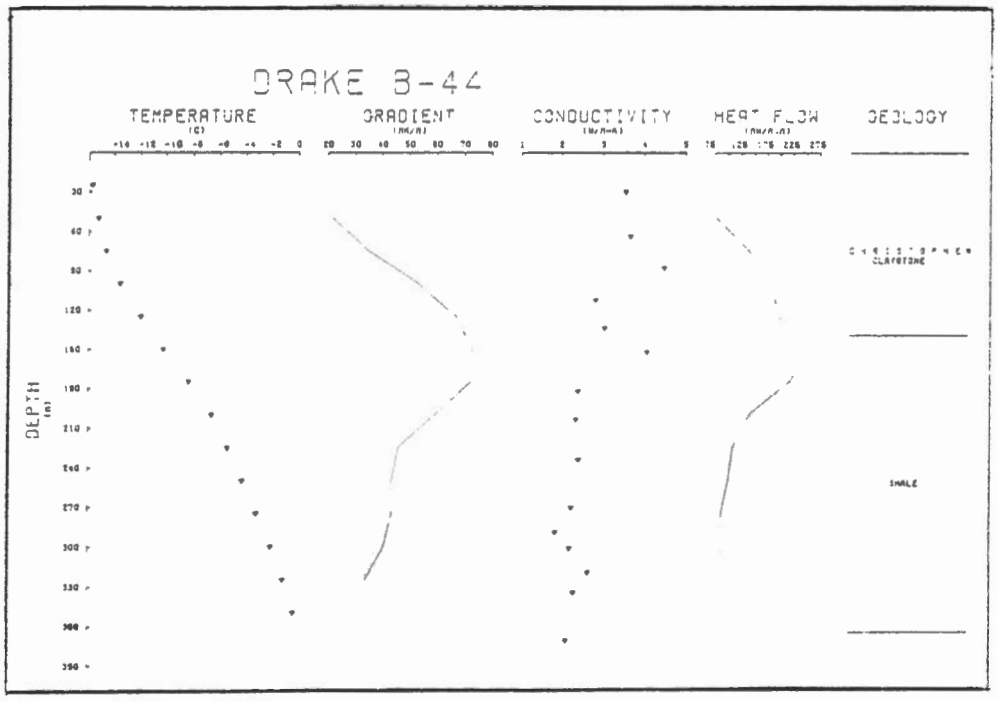

Figure B-2. Corrected heat flow for topography.

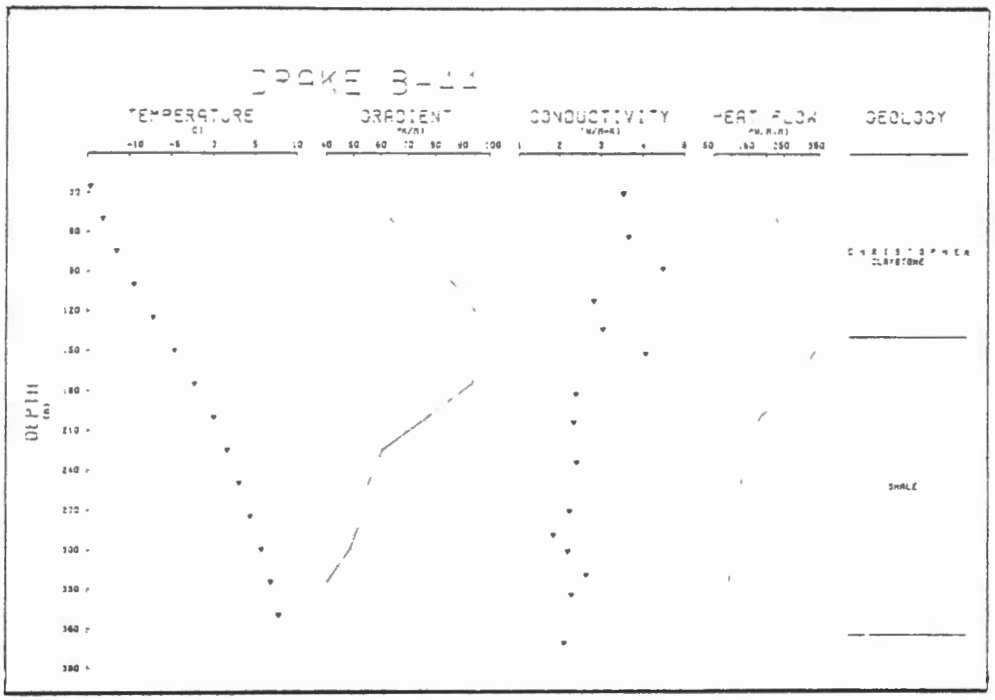

Figure B-3. Corrected heat flow for moving shoreline.

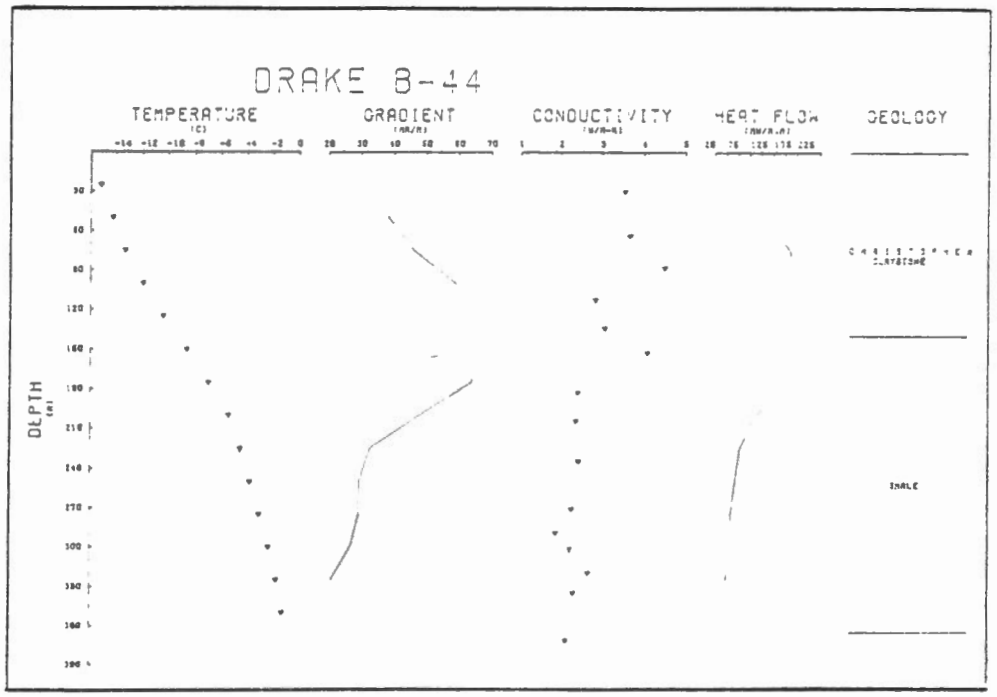

Figure B-4. Corrected heat flow for climatic history.

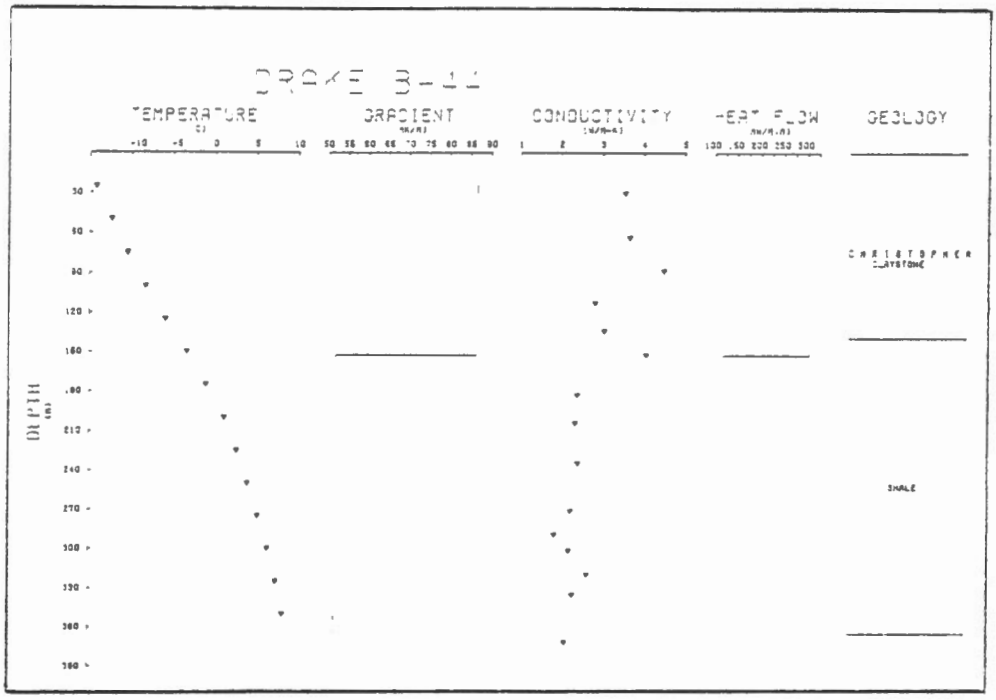

Figure B-5. Uncorrected heat flow per formation.

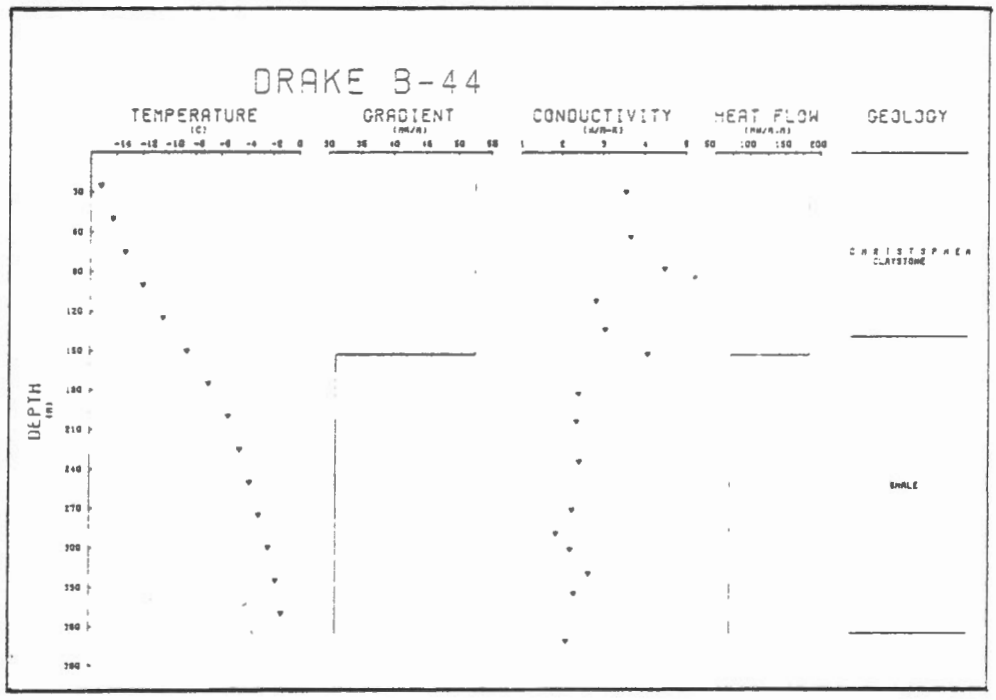

Figure B-6. Corrected heat flow for climatic history per formation.

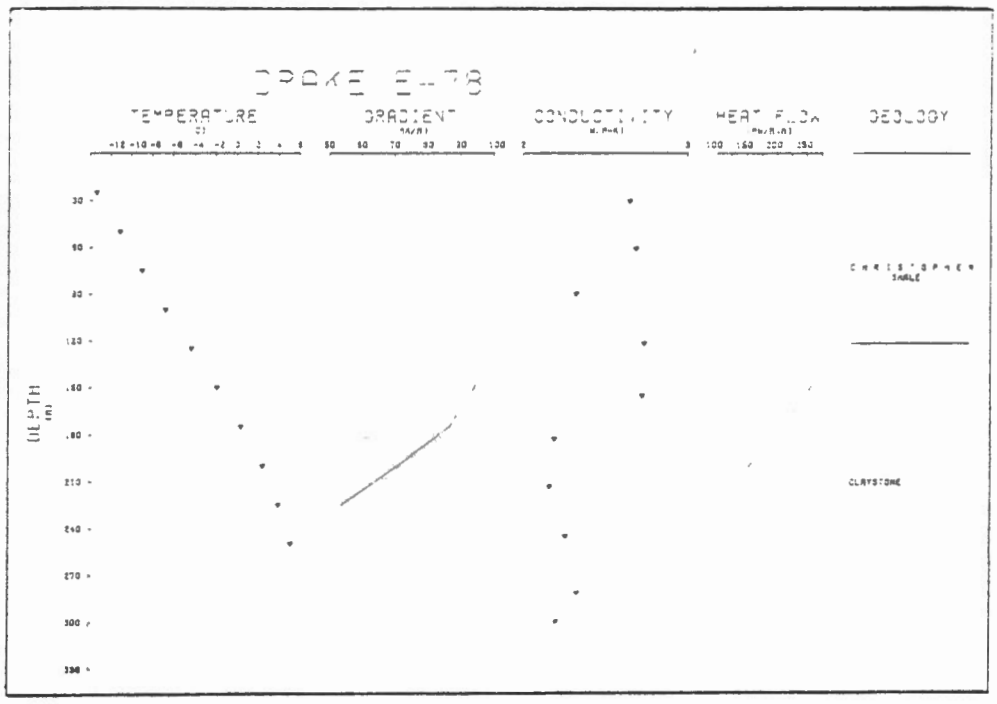

Figure B-7. Uncorrected heat flow.

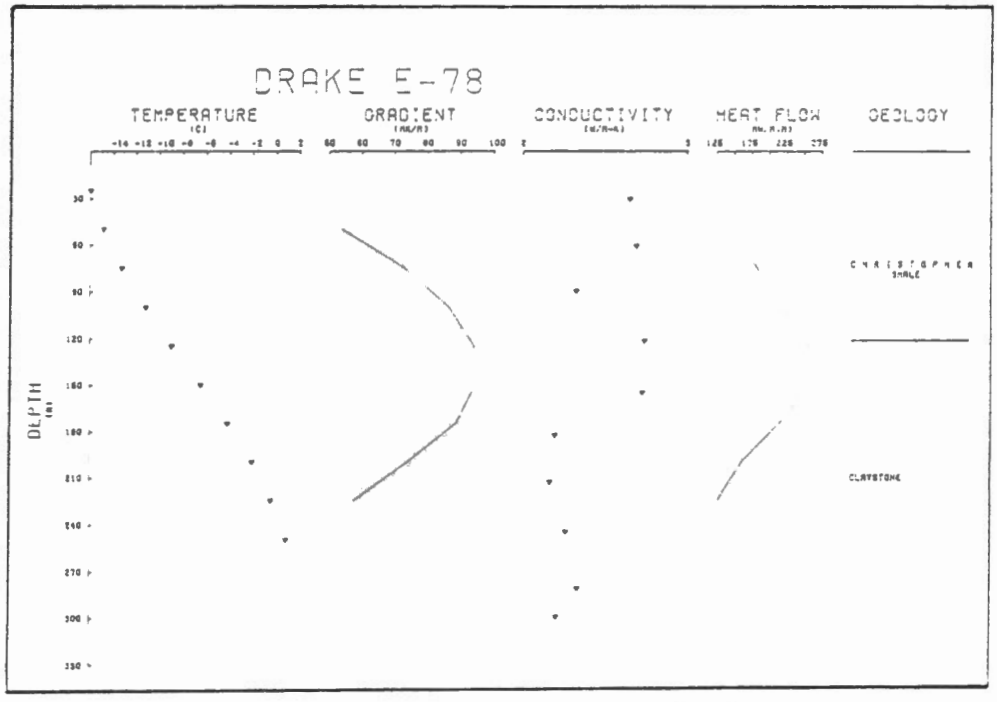

Figure B-8. Corrected heat flow for topography.

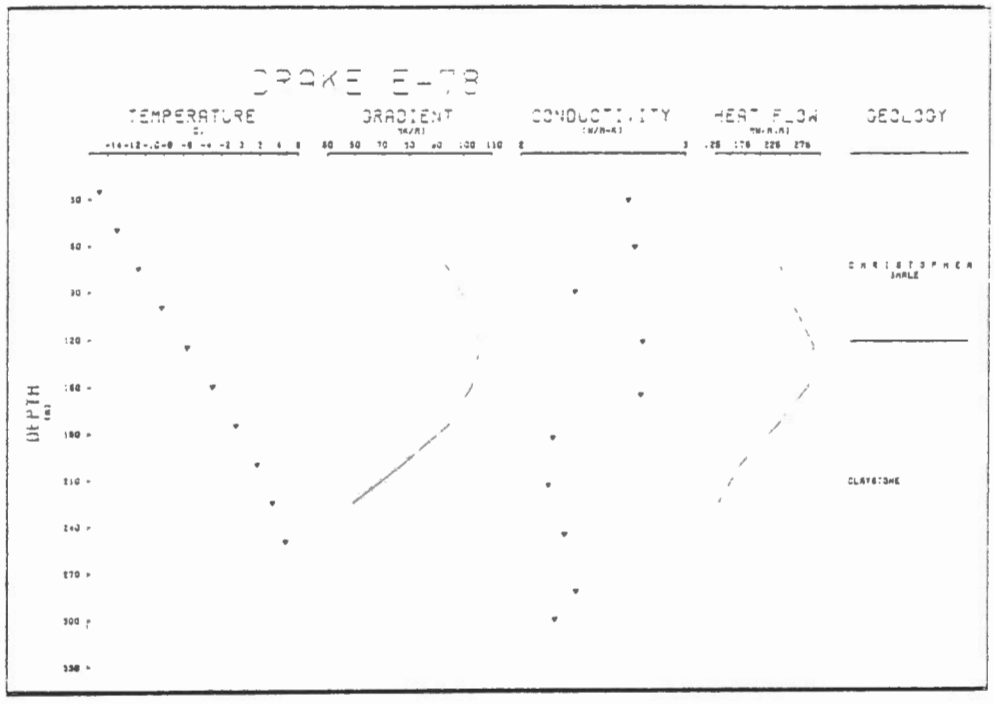

Figure B-9. Corrected heat flow for moving shoreline.

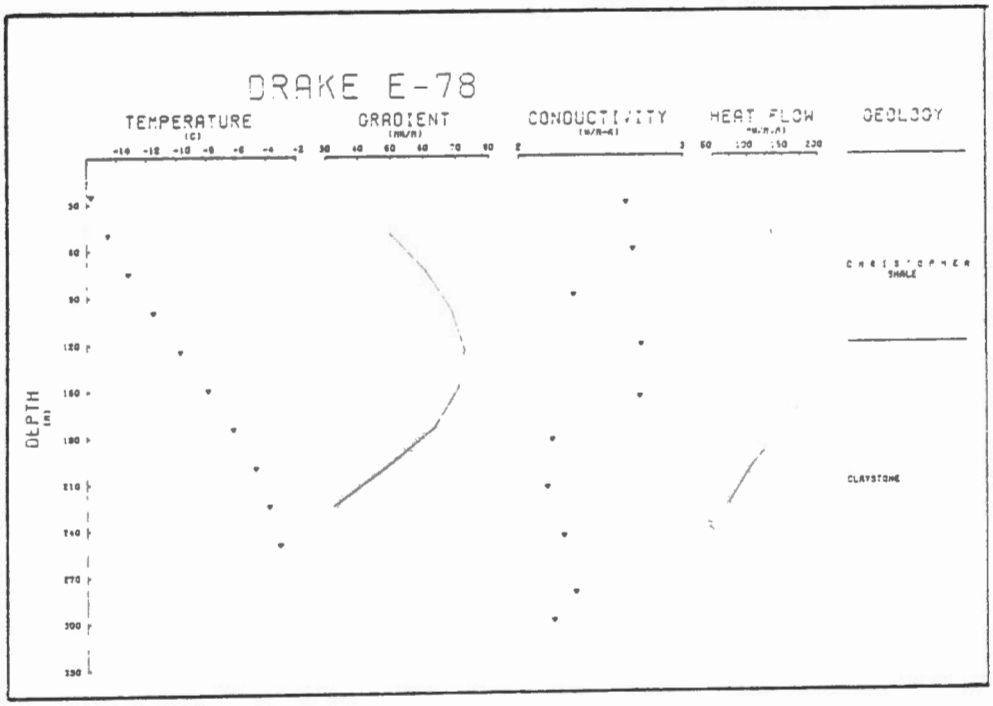

Figure B-10. Corrected heat flow for climatic history.

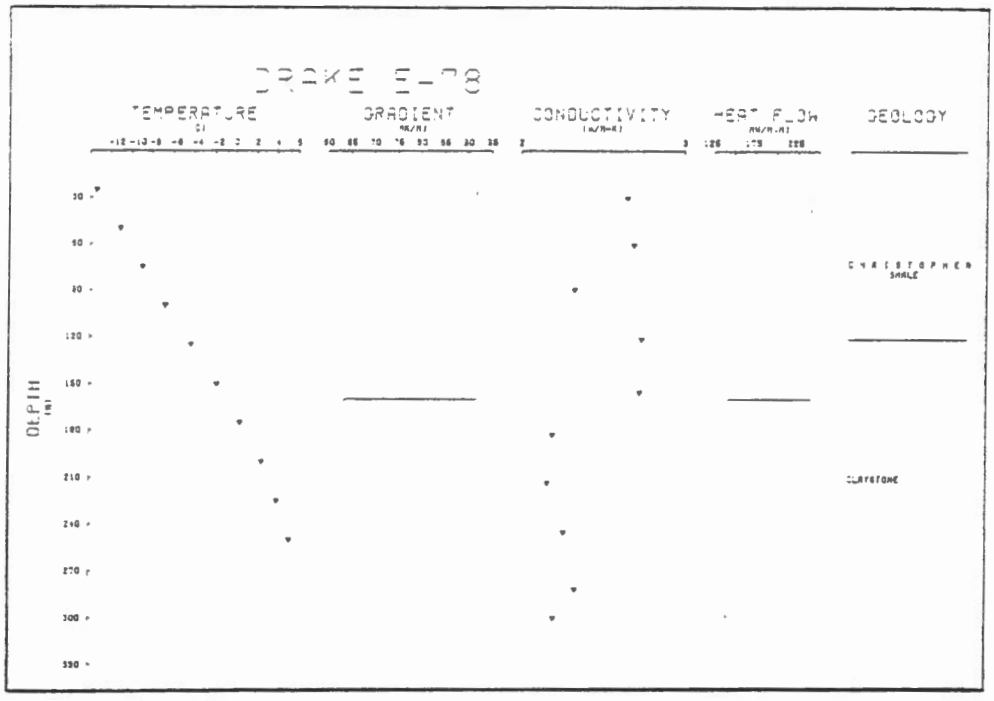

Figure B-11. Uncorrected heat flow per formation.

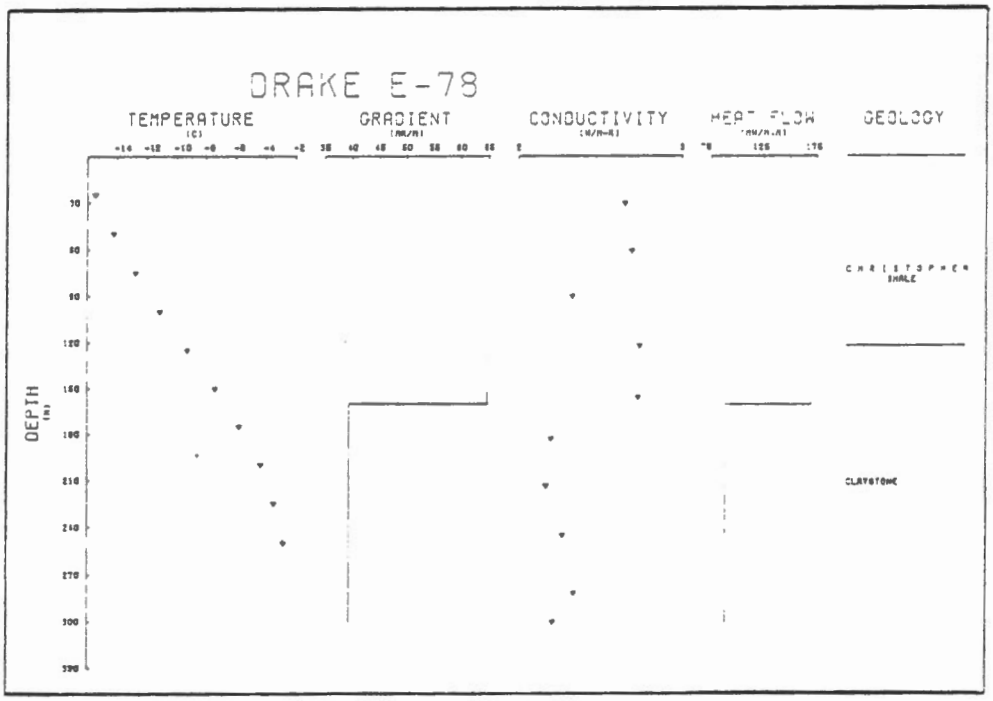

Figure B-12. Corrected heat flow for climatic history per formation.

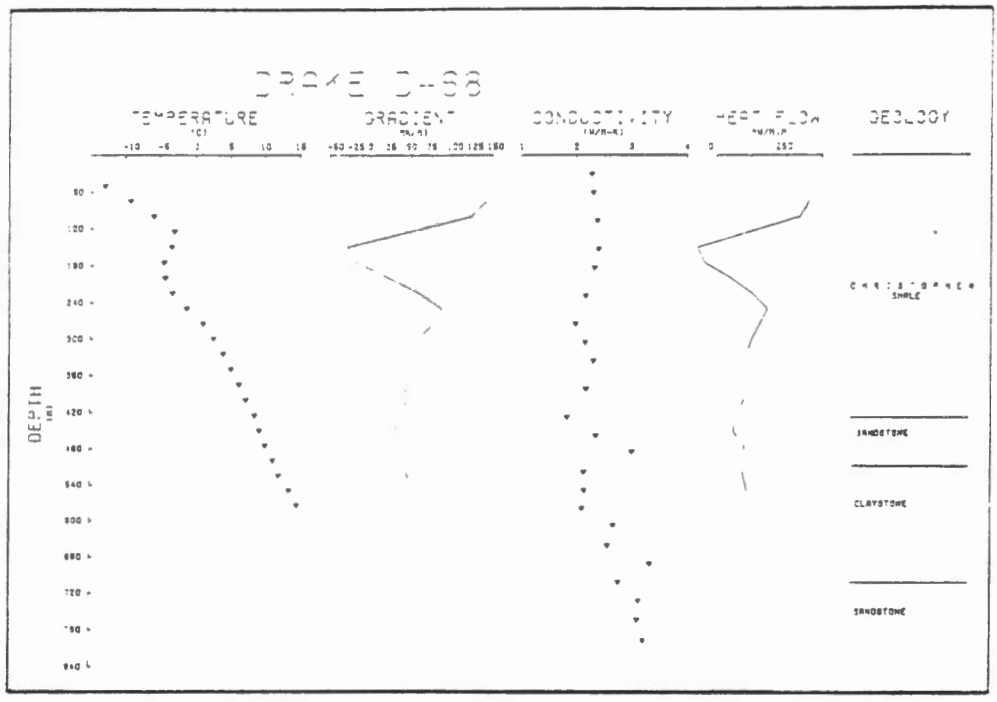

Figure B-13. Uncorrected heat flow.

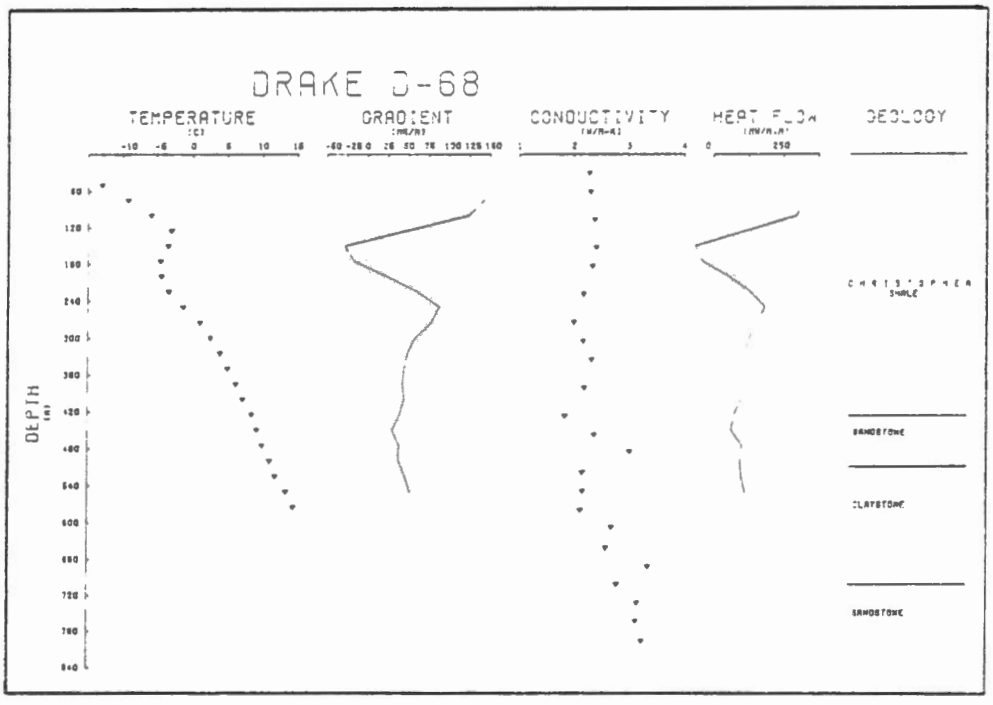

Figure B-14. Corrected heat flow for topography.

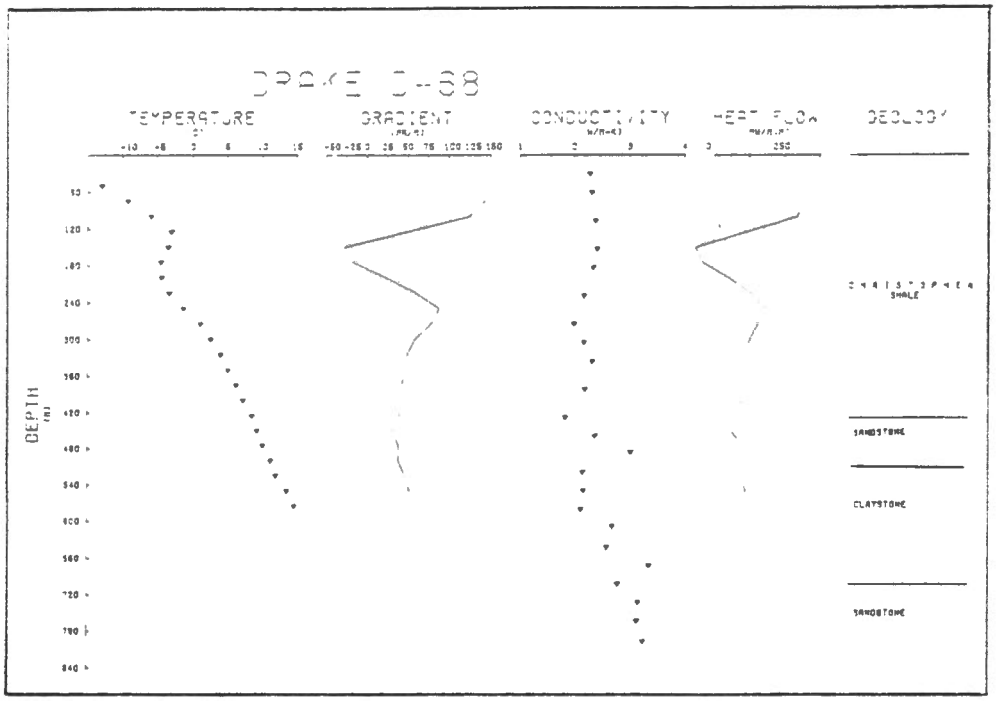

Figure B-15. Corrected heat flow for moving shoreline.

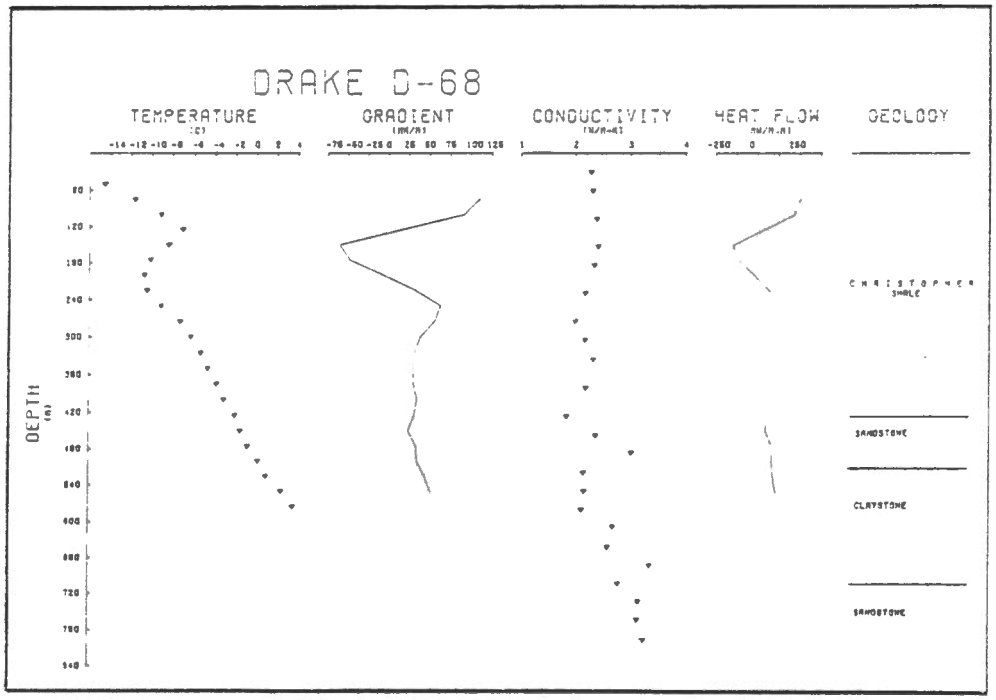

Figure B-16. Corrected heat flow for climatic history.

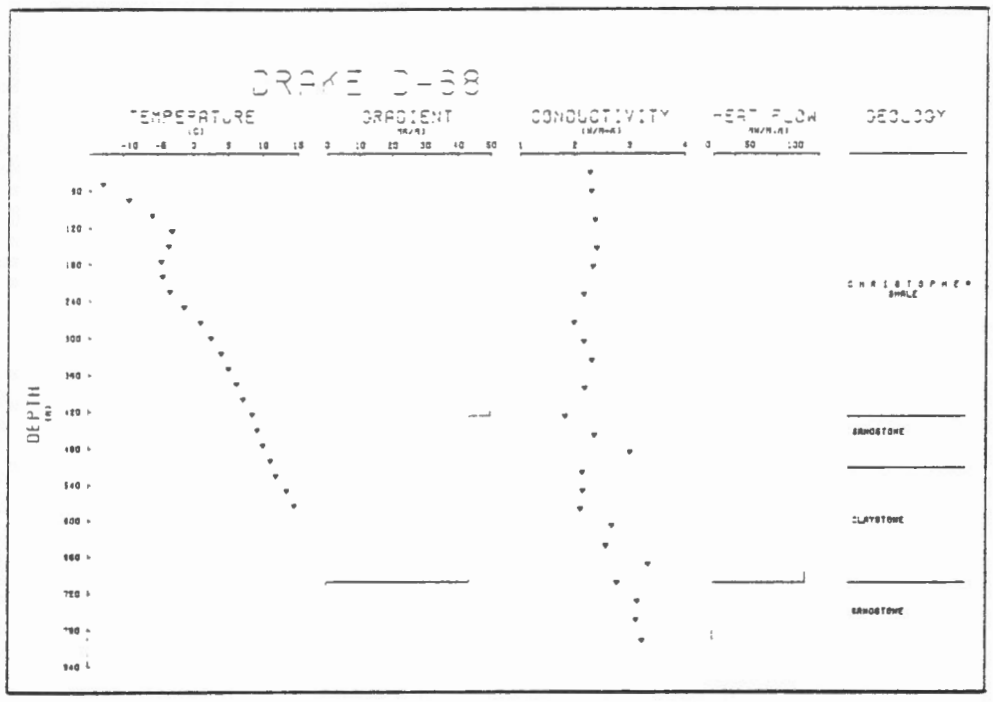

Figure B-17. Uncorrected heat flow per formation.

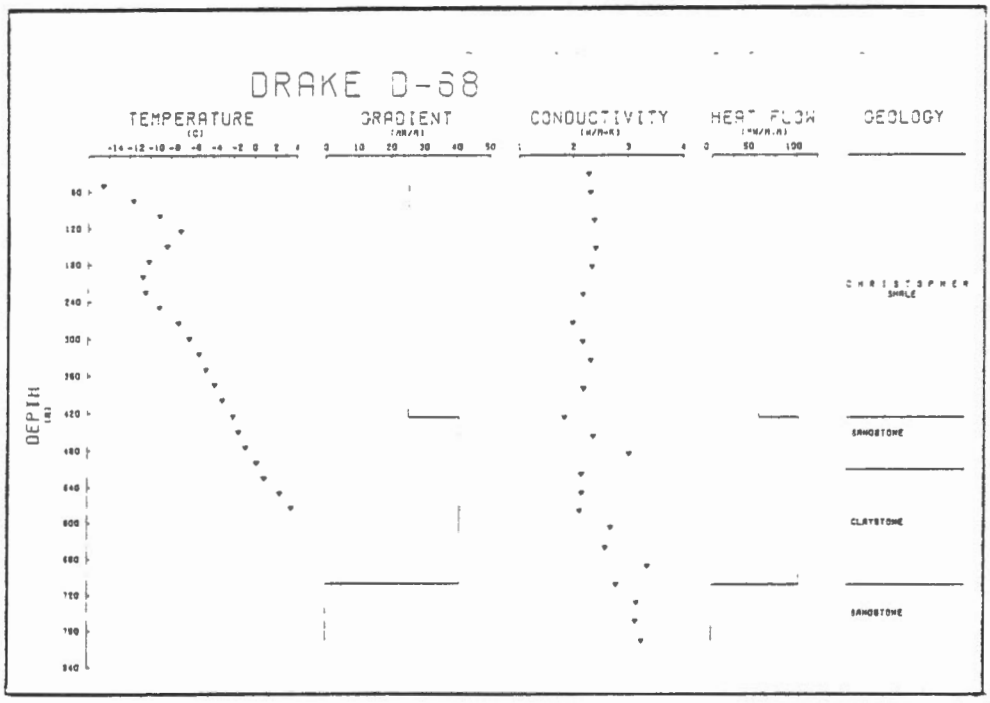

Figure B-18. Corrected heat flow for climatic history per formation.

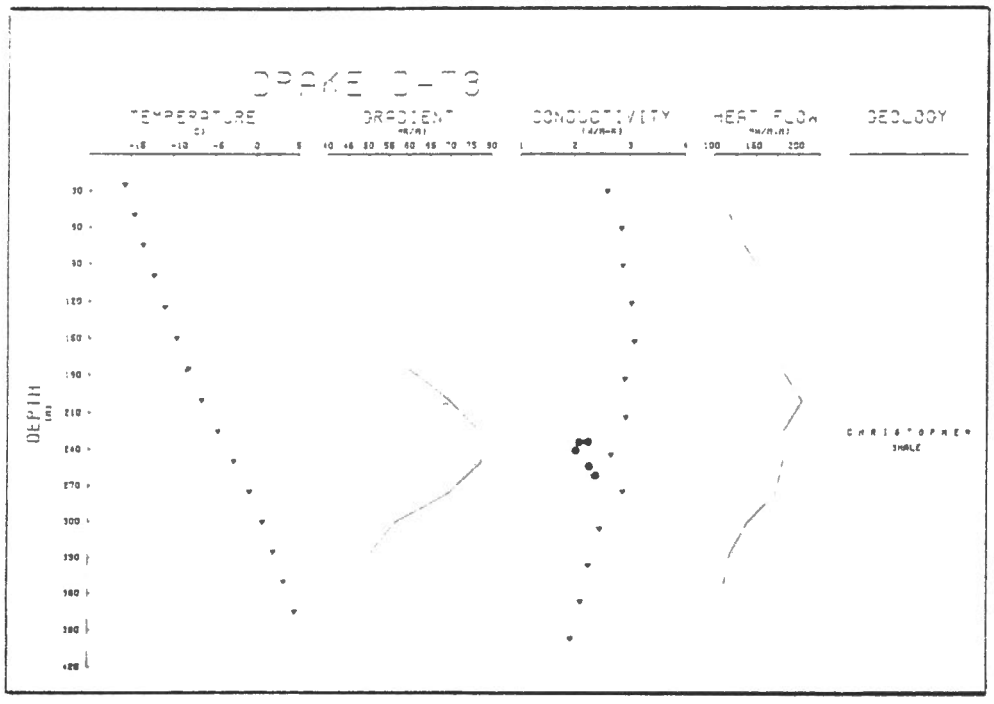

Figure B-19. Uncorrected heat flow.

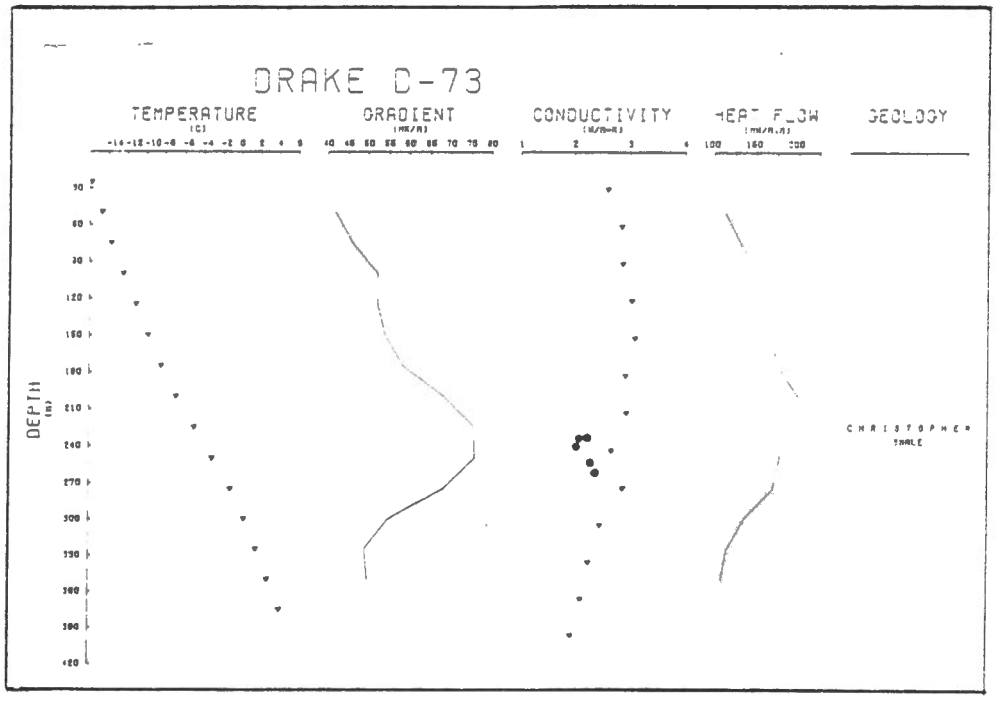

Figure B-20. Corrected heat flow for topography.

• assumed values

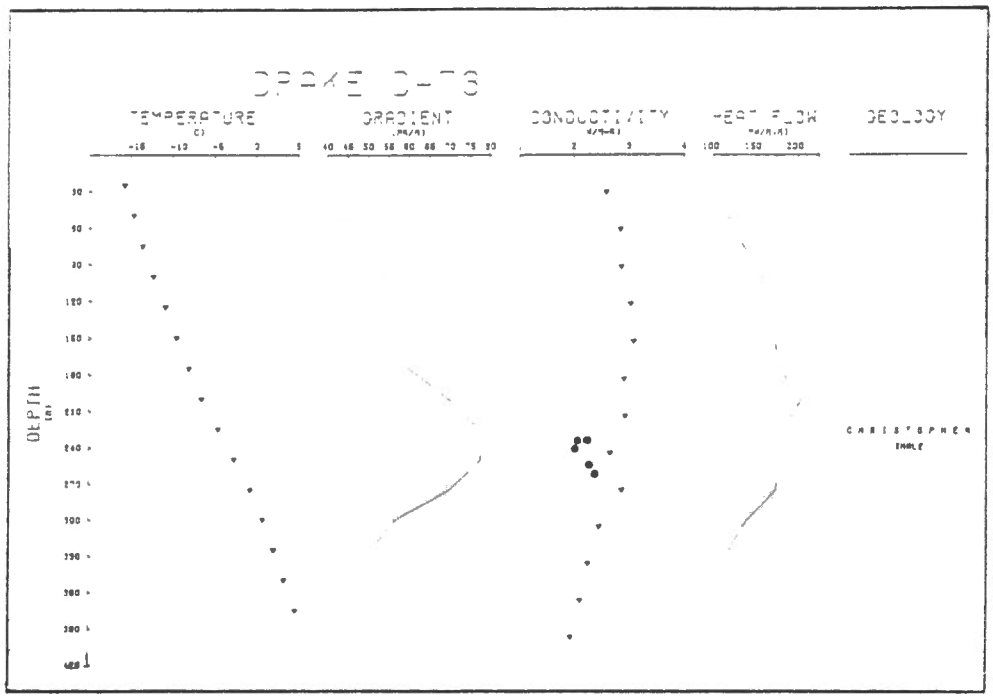

Figure B-21. Corrected heat flow for moving shoreline.

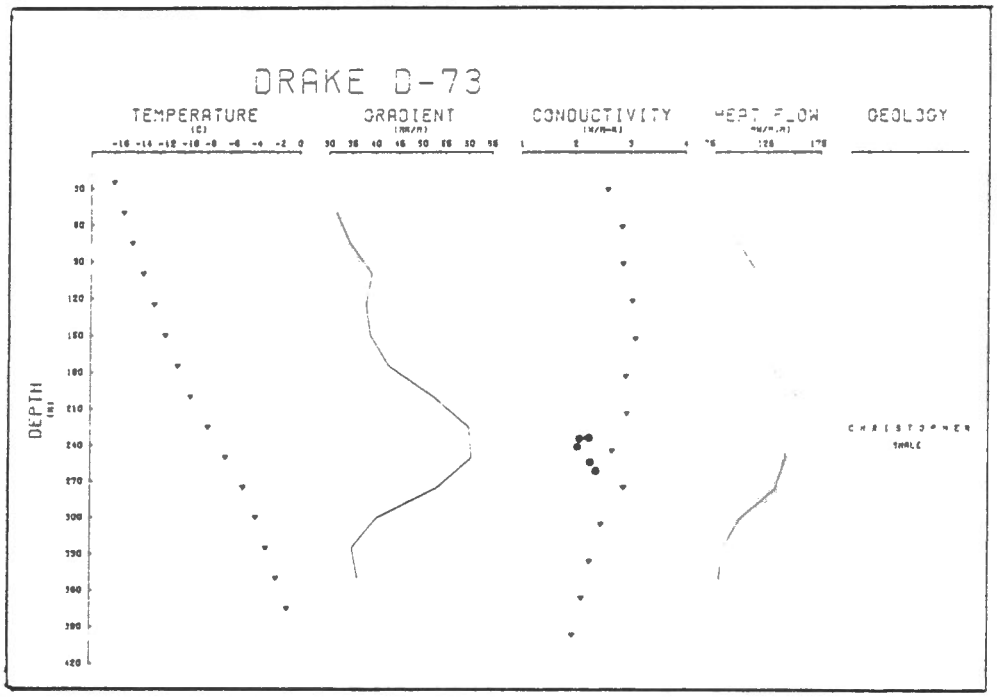

Figure B-22. Corrected heat flow for climatic history.

• assumed values

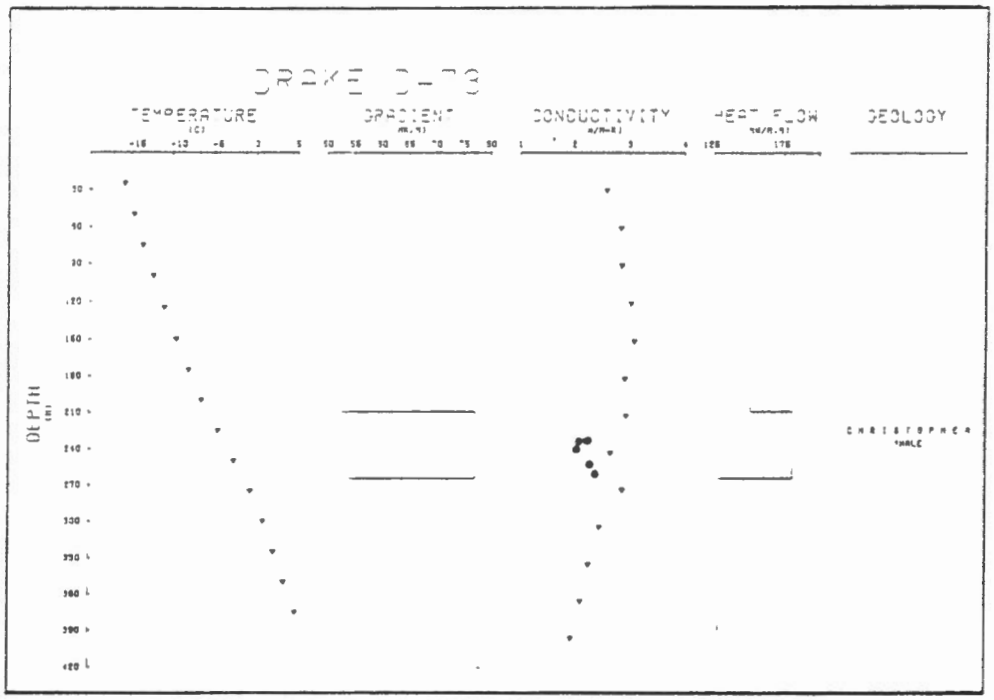

Figure B-23. Uncorrected heat flow per formation.

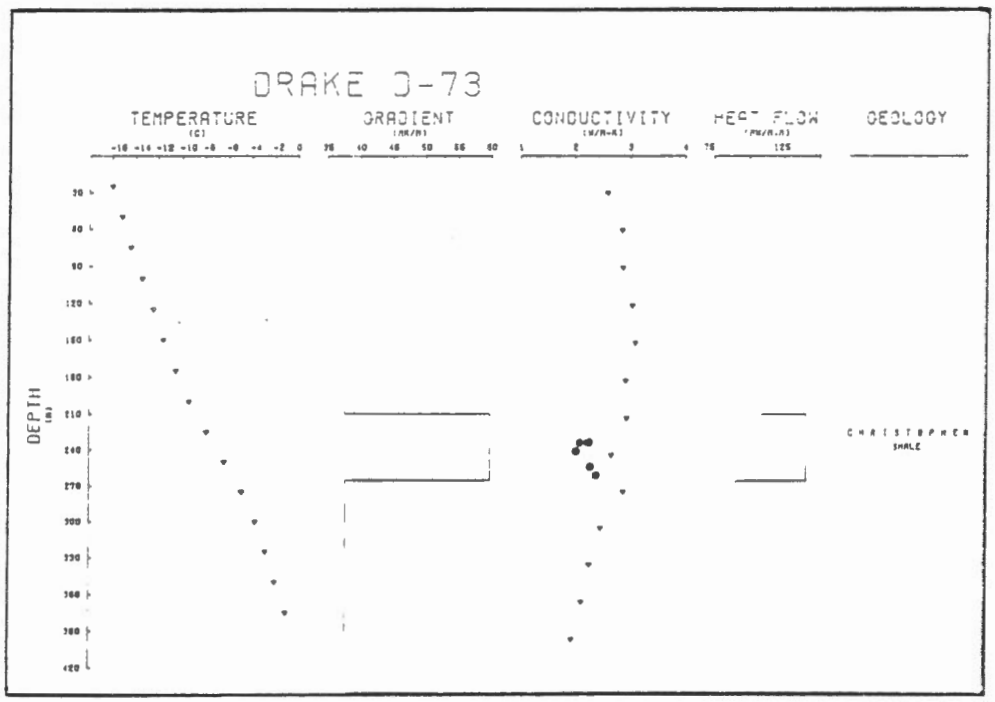

Figure B-24. Corrected heat flow for climatic history per formation.

• assumed values

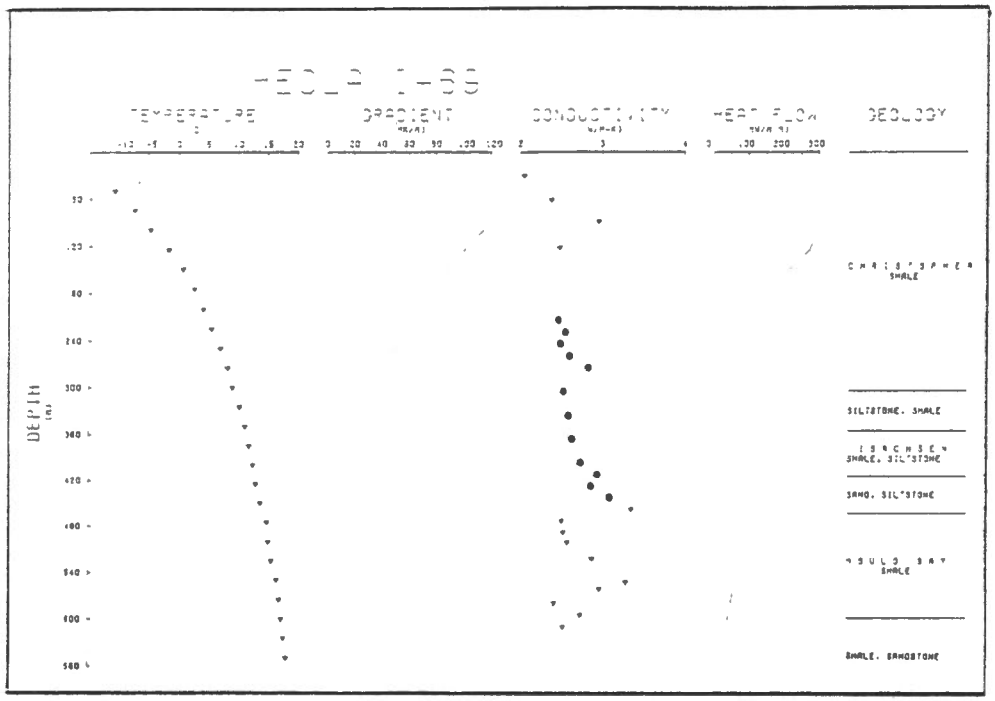

Figure B-25. Uncorrected heat flow.

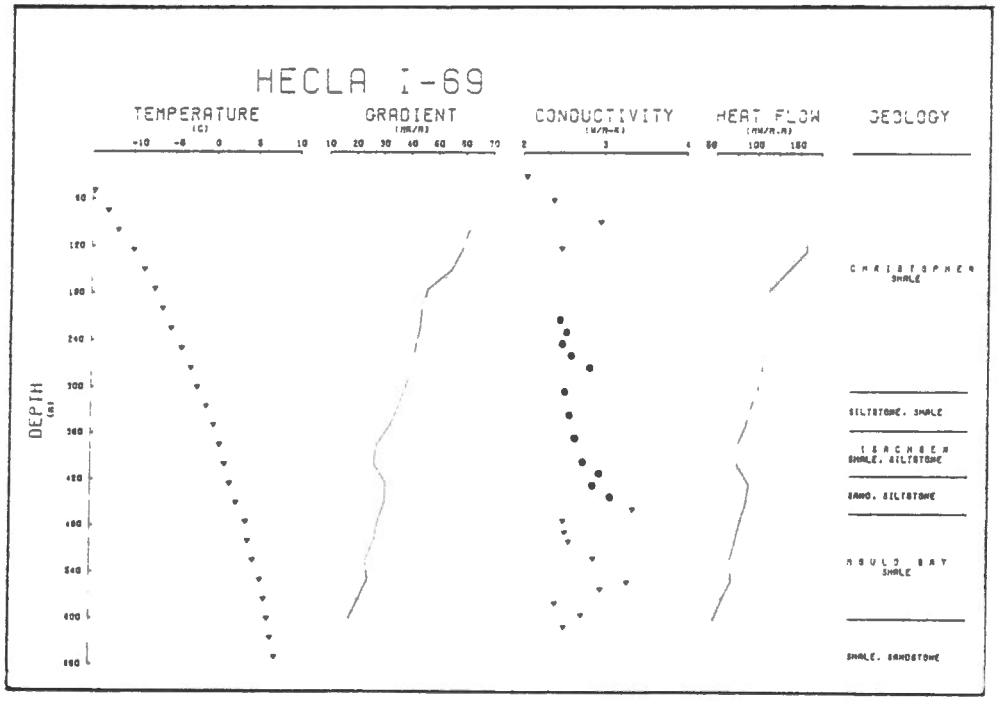

Figure B-26. Corrected heat flow for topography.

• assumed values

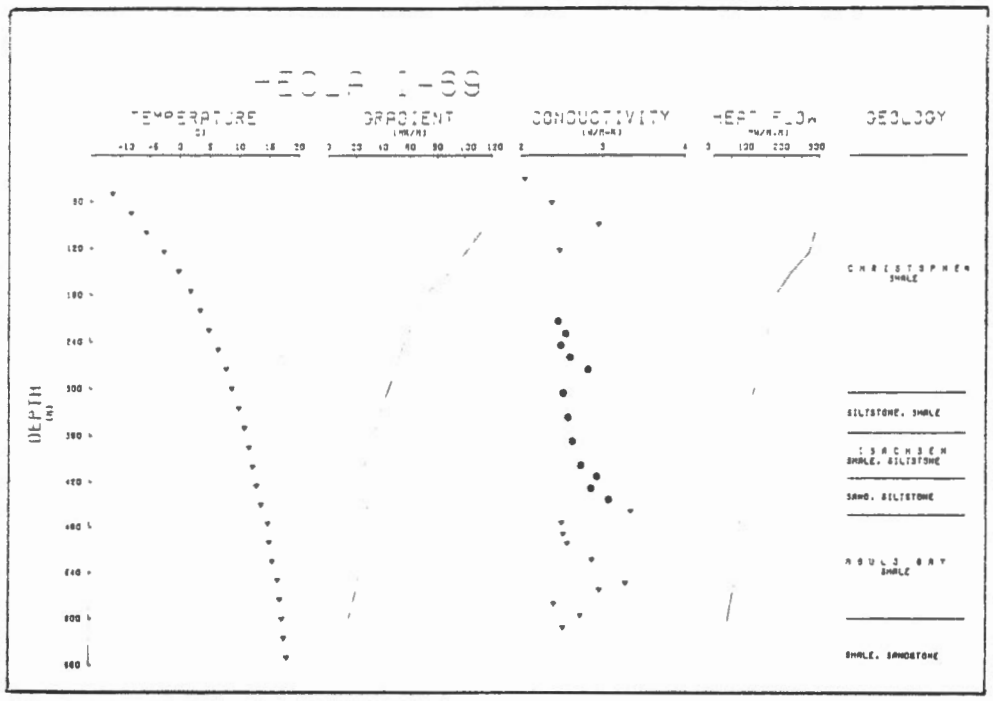

Figure B-27. Corrected heat flow for moving shoreline.

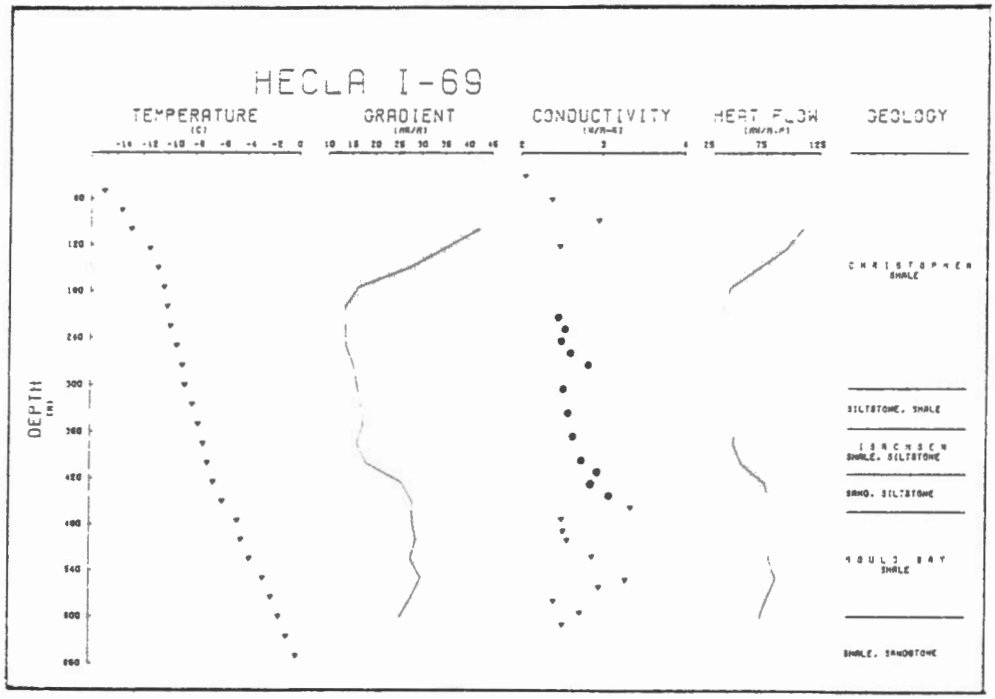

Figure B-28. Corrected heat flow for climatic history.

• assumed values

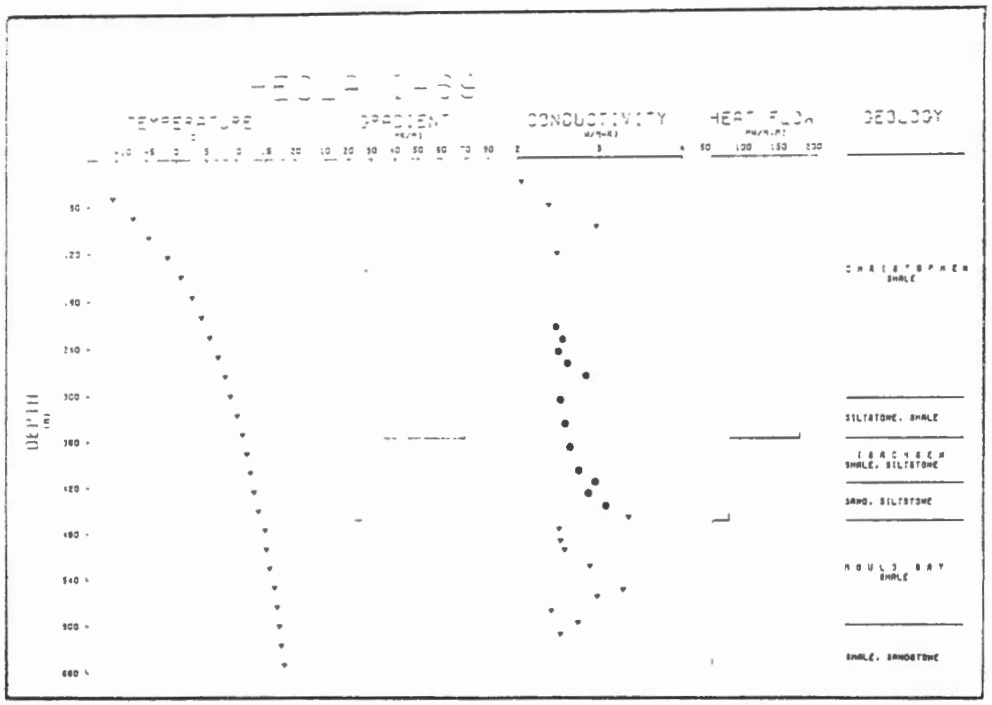

Figure B-29. Uncorrected heat flow per formation.

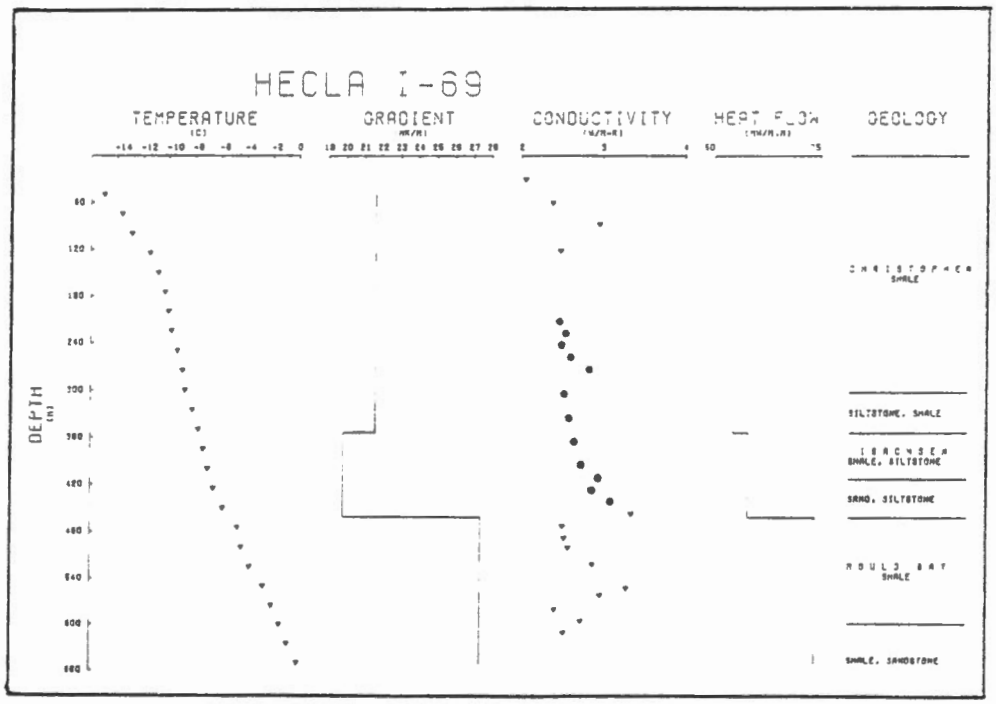

Figure B-30. Corrected heat flow for climatic history per formation.

• assumed values